ACS APPLIED MATERIALS & INTERFACES

Review

www.acsami.org

Synthesis and Application of Colloidal $CuInS_2$ Semiconductor Nanocrystals

Joanna Kolny-Olesiak[‡,*] and Horst Weller[†]

[‡]Energy and Semiconductor Research Laboratory, Department of Physics, Carl von Ossietzky University of Oldenburg, 26129 Oldenburg, Germany

[†]Institute of Physical Chemistry, University of Hamburg, Grindelallee 117, 20146 Hamburg, Germany

ABSTRACT: Semiconductor nanocrystals possess size-dependent properties, which make them interesting candidates for a variety of applications, e.g., in solar energy conversion, lighting, display technology, or biolabelling. However, many of the best studied nanocrystalline materials contain toxic heavy metals; this seriously limits their potential for widespread application. One of the possible less toxic alternatives to cadmium- or lead-containing semiconductors is copper indium disulfide (CIS), a direct semiconductor with a bandgap in the bulk of 1.45 eV and a Bohr exciton radius of 4.1 nm. This Review gives an overview of the methods developed during the last years to synthesize CIS nanocrystals and summarizes the possibilities to influence their shape, composition and crystallographic structure. Also the potential of the application of CIS nanocrystals in biolabellling, photocatalysis, solar energy conversion, and light-emitting devices is discussed.

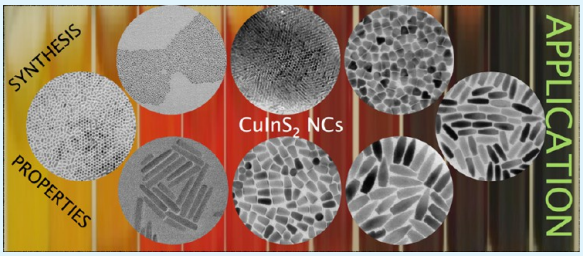

KEYWORDS: *nanocrystals, colloidal synthesis, I–III–VI semiconductors*

INTRODUCTION

Development of new materials is a major driving force of technological evolution. During the last two decades, immense progress has been achieved in the fabrication and manipulation of nanoscale crystallites and in the understanding of their size and shape dependent characteristics.[1−7] This extends our means to produce custom-made materials for specific applications: the properties of nanomaterials can be adjusted not only dependent on their chemical composition but also on their geometrical parameters. For instance, the bandgap of a semiconductor, which is a material specific constant for a bulk material, depends on the size of the nanocrystallites. Thus, we can influence the optical properties of semiconductor materials in the nanometer range, by controlling their size. This can be achieved by wet-chemical synthetic methods, which usually yield colloidal solutions of inorganic particles stabilized by an organic ligand shell. Adjusting parameters of the synthesis such as temperature, concentration and nature of precursors and solvents allows for a fine-tuning of the composition, size and shape of the resulting nanocrystals. Especially in the case of binary materials, such as II–VI or IV–VI semiconductors, a vast amount of synthetic procedures allowing for precise size and shape control has been developed and a number of studies were conducted in recent years, which shed light on the underlying reaction mechanisms of the nanocrystals formation and growth.[8−16] The excellent and precisely controllable optical properties of cadmium chalcogenide nanocrystals have already enabled their application in commercially available displays with high color purity. However, the best studied II–VI and IV–VI semiconductors have a severe drawback, which strongly restricts their large scale application: they contain highly toxic heavy metals, cadmium, and lead. Less toxic materials, which possess similar optical properties, can be found among ternary I–III–VI semiconductors (Figure 1).[17−19] Copper indium disulfide (CIS), for instance, is a direct semiconductor with a bulk bandgap of 1.45 eV, high extinction coefficient in the visible spectral range, exceptional radiation hardness, and pronounced defect tolerance. Therefore, increasing activity can be observed in the field of the colloidal synthesis of $CuInS_2$ nanocrystals, resulting from the hope to develop alternative

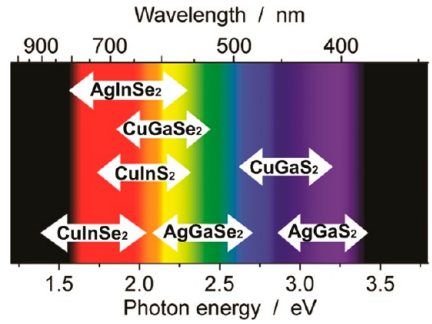

Figure 1. Optical bandgap for I–III–VI nanocrystals in the size range between 2 and 5 nm. Reprinted with permission from ref 20. Copyright 2009 AIP Publishing.

Received: September 20, 2013
Accepted: November 4, 2013
Published: November 4, 2013

nanocrystalline materials for applications in solar energy conversion, photodetectors, light-emitting devices, photocatalysis, or biomedical applications. The synthesis of ternary materials requires, however, adjusting the reactivity of two cationic precursors at the same time, which makes finding optimum reaction conditions and avoiding the formation of undesired side-products more complicated, than in the case of binary compounds. Furthermore, CIS frequently differs from the exact 1:1:2 ratio between copper, indium and sulfur; thus, the stoichiometry of the nanoparticles is an additional parameter, which can be adjusted by changing the conditions of the synthesis and can be used to fine-tune the properties of the resulting material. Different strategies, which have been developed to control the size, shape, composition and crystallographic structure of CIS nanoparticles are summarized in this Review. Furthermore, the application of CIS nanocrystals in biolaballing, photocatalysis, solar energy conversion, and light-emitting diodes are discussed.

1. Properties of $CuInS_2$ Nanocrystals. CIS is a direct semiconductor with a bandgap of 1.45 eV and high extinction coefficients in the visible spectral range, which makes it an interesting material for application in solar energy conversion. The Bohr exciton radius of CIS is 4.1 nm, thus, quantum confinement effects can be observed in CIS nanocrystals up to a size of about 8 nm. By changing the sizes of CIS nanoparticles, their absorption and emission can be tuned almost in the whole visible part of the solar spectrum, up to the near infrared (Figure 2). Finite-depth-well effective mass approximation

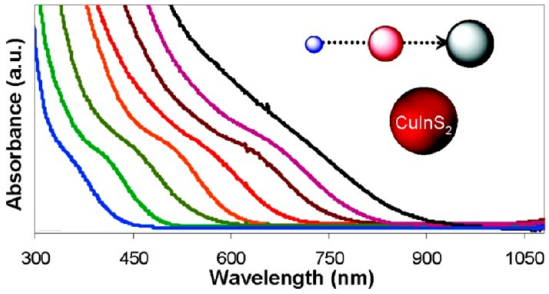

Figure 2. Absorption spectra of CIS nanocrystals of different sizes between 2 and 16 nm. Adapted with permission from ref 23. Copyright 2009 American Chemical Society.

calculations conducted for CIS nanocrystals with chalcopyrite structure in the size range between 1 and 6 nm show that their bandgap can be tuned between 3.3 and 1.7 eV,[20] which is in good agreement with the experimental data for this size range (Figure 2).

Not only the size but also the composition can influence the bandgap of CIS nanocrystals.[21] The valence band of CIS, which is composed of Cu 3d and S 3p orbitals, is lowered in copper deficient particles. Thus, the bandgap is widened in Cu poor CIS nanocrystals (Figure 3).[21,22]

The absorption spectrum of CIS nanocrystals does not exhibit a sharp excitonic peak, in fact, only a more or less pronounced shoulder can be observed (see Figure 2). There are several potential explanations for this fact. This could be an intrinsic property of CIS nanocrystals or originate from inhomogeneities within the studied samples, regarding the size, the shape or the composition. In spite of the progress achieved in the last decade in the synthesis of CIS nanocrystals, most of the methods developed so far yield particles with rather

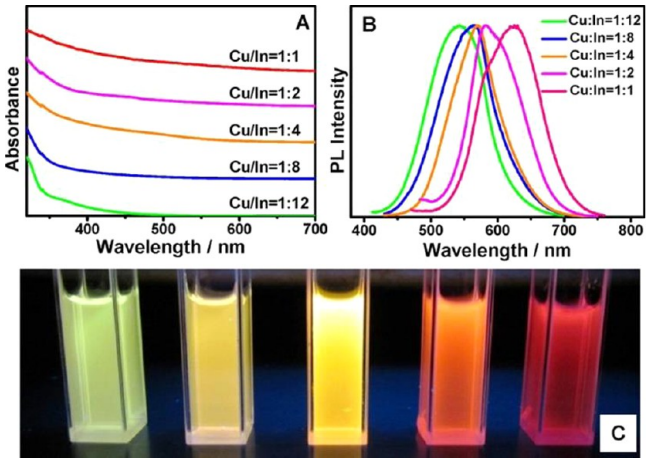

Figure 3. (a) Absorption and (b) fluorescence spectra of CIS nanoparticles with different Cu:In ratio and (c) a picture of the corresponding solutions under UV irradiation. Reprinted with permission from ref 40. Copyright 2013 American Chemical Society.

broad size or shape distribution (see section 2), which complicates studying the size- or shape-dependent optical properties of this material. The size distribution of CIS nanocrystals can be narrowed by size selective precipitation. Xie et al.[23] achieved an improvement of the optical properties and could observe a well-defined excitonic peak and a narrower photoluminescence band in a size selected sample. In contrast to these results, Castro et al.[24] did not observe more distinct features in the absorption spectrum after size selective precipitation; the full-width-at-half-maximum (FWHM) of the emission spectrum was not affected.

Another feature usually observed in the absorption spectrum of CIS nanocrystals is a tail on the low energy side of the spectrum (Figure 2). This could originate from the participation of the electronic states of the surface ligands in the absorption, or could be a contribution of intraband states of CIS. Castro et al.[24] studied the influence of different ligands on the optical properties of CIS nanocrystals and found that the shape of the absorption spectrum is not affected by surface ligands. Thus, the contribution of the intraband states seems to be responsible for the shape of the absorption spectra of CIS nanocrystals.

The knowledge of the concentration of a nanocrystals solution is essential for many applications. This information can be easily obtained from the measurement of the absorption in the UV−vis region, if the extinction coefficient is known. The extinction coefficients of nanocrystalline materials depend on the size of the crystallites, thus, they have to be determined for different diameters of the nanoparticles. Furthermore, the dependence of the position of the absorption features (maximum or shoulder) from the size of the nanocrystals must be known.

There are two reports about the determination of the size-dependent extinction coefficients for CIS nanocrystals and CIS-ZnS core-shell structures.[25,26] Booth et al.[25] determined of the size dependent molar extinction coefficients at the wavelength of the first excitonic transition ($\varepsilon_{CIS}(E_1)$, eq 1), which was found from the local minimum of the second derivative of the absorption spectrum, and at 3.1 eV (ε_{CIS}(3.1 eV), eq 2). Because of the relatively high optical density (compared to the value at the wavelength of the first electronic transition), using the absorption at this energy has the advantage of higher

sensitivity. Furthermore, there is no influence of the ligands or a ZnS shell, and thus, the measurement of the concentration of the nanocrystals is independent from their surface properties and reflects only the concentration of the CIS core.

$$\varepsilon_{CIS}(E_1) = (830 \pm 660)d^{3.7\pm0.6} \quad (1)$$

$$\varepsilon_{CIS}(3.1\ \text{eV}) = (2123 \pm 109)d^{3.8\pm0.3} \quad (2)$$

Qin et al.[26] used another method to find the wavelength of the first excitonic transition; they took the position of the intersection of two tangents in the absorption spectrum. They determined the size dependent extinction coefficients for both $CuInS_2$ ($\varepsilon_{CIS}(E_1)$, eq 3) and $ZnCuInS_3$ ($\varepsilon_{ZCIS}(E_1)$, eq 4). The values found in this study for CIS are slightly lower, than extinction coefficients reported for other nanocrystalline materials. $ZnCuInS_3$ was found to have higher extinction coefficients than $CuInS_2$, which the authors of the study explained with the fact, that ZnS has higher extinction coefficients than $CuInS_2$. However, their assumption that the molar extinction coefficients of an alloy compound could be estimated from the extinction coefficients of its components ($CuInS_2$ and ZnS in this case) still has to be verified.

$$\varepsilon_{CIS}(E_1) = 11430d^{2.147} \quad (3)$$

$$\varepsilon_{ZCIS}(E_1) = 11000d^{2.8018} \quad (4)$$

The extinction coefficients obtained in both studies show similar size dependence in the examined size range (~2.5 to 6 nm); however, the values calculated with eqs 1 and 3 differ significantly. The reason for this discrepancy is most likely related to the relatively broad size distribution of the samples used in both studies, as well as to the not-spherical shape of the nanoparticles, which complicated the exact determination of the size. Furthermore, the almost featureless absorption spectra of CIS nanocrystals make it difficult to assign unambiguously the position of the first excitonic transition. Therefore, further progress in the development of synthetic methods is needed to obtain more reliable extinction coefficients for CIS nanoparticles.

Apart from the absorption in the visible spectral region, CIS particles can exhibit localized surface plasmon resonance bands in the NIR (Figure 4).[27] Free charge carriers giving rise to this absorption are holes, which are present in the particles because of cation deficiencies. The presence of plasmon resonance in a semiconducting material is of interest for applications, for example, in photovoltaics, because of the possibility to near-field coupling of the plasmonic resonance to electronic excited states.

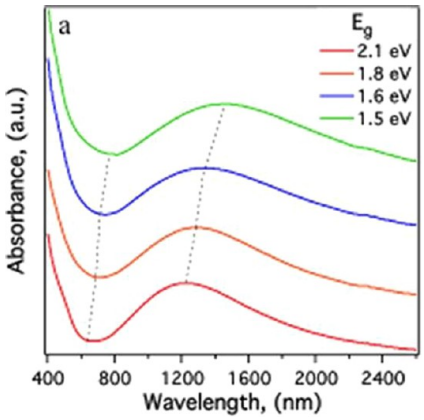

Figure 4. Absorption spectra of CIS nanocrystals with different bandgaps and positions of the plasmon band. Adapted with permission from ref 27. Copyright 2012 American Chemical Society.

Absorption of light results in the generation of excited charge carriers, which can recombine upon emission of light (Figure 5). This process is relatively inefficient in pure CIS nanocrystals; quantum yields in order of magnitude of 1% are frequently reported for this material. All the studies of the emission properties of CIS nanoparticles report broad photoluminescence (PL) features with full-width-at-half-maximum (FWHM) of about 100 nm; sometimes the emission spectrum is composed of two or three overlapping bands.[28] Furthermore, the Stokes shift is relatively large (130−170 nm) and the decay times measured by time-resolved photoluminescence spectroscopy are in the order of magnitude of several hundreds of nanoseconds. All these characteristics differ from that expected for band edge emission, which suggests that the surface and defect trap states are involved in the emission process, rather than the recombination of electron and holes in the quantized conduction and valence bands.

Several studies assign the emission of CIS nanocrystals to a donor−acceptor (D−A) transition.[21,22,24,29] Li et al.[28] studied the time dependence of the PL of CIS nanoparticles and observed a red shift of the emission bands with the delay time. This is expected for D−A pair recombination and originates from the contribution of the Coulomb energy, which decreases, whereas the separation between the donor and the acceptor increases. Copper vacancy is believed to be the acceptor state, whereas sulfur vacancy or copper indium substitution act as the donor.[24] Therefore, increasing the amount of copper vacancies can be an efficient way to increase the emission quantum yield. Uehara et al.[21] achieved an increase in the quantum yield by deliberately introducing copper vacancies into their CIS nanocrystals; the sample with the composition $CuIn_{2.3}S_4$ had the maximum quantum yield of 5%, whereas no photoluminescence could be observed from the particles with the composition 1:1:2. Also, in other studies, an increase of the quantum yield was observed with increasing copper deficiency.[22,30]

Hamanaka et al.,[31] who studied the origin of the emission in 2 nm copper-rich CIS nanoparticles (Cu:In:S = 1.52:1:2.96), assign the photoluminescence to the recombination of electrons and holes trapped in the deep surface defect states, rather than to a D−A transition between intrinsic defects. The PL decay times were 30 and 260 ns, depending on the emission energy, however, no dependence of the position of the PL band with excitation energy was observed, which would be typical for D−A pair PL. The emission properties of the particles used in this study were, furthermore, very sensitive to species of the surfactants present on the surface of the nanoparticles, which supports the assumption that surface trap states are involved in the emission process.

Combining CIS nanoparticles with other compounds, such as ZnS, CdS, $CuGaS_2$, or $CuInSe_2$, is an effective means to adjust the optical properties of this material. Covering CIS nanocrystals with a shell of a semiconductor with a larger bandgap reduces the amount of surface traps and the related nonradiative recombination of photogenerated charge carriers, and thus increases the photoluminescence quantum yield of the particles (Figure 5c). By alloying CIS with compounds having larger bandgaps, the absorption of CIS nanocrystals can be

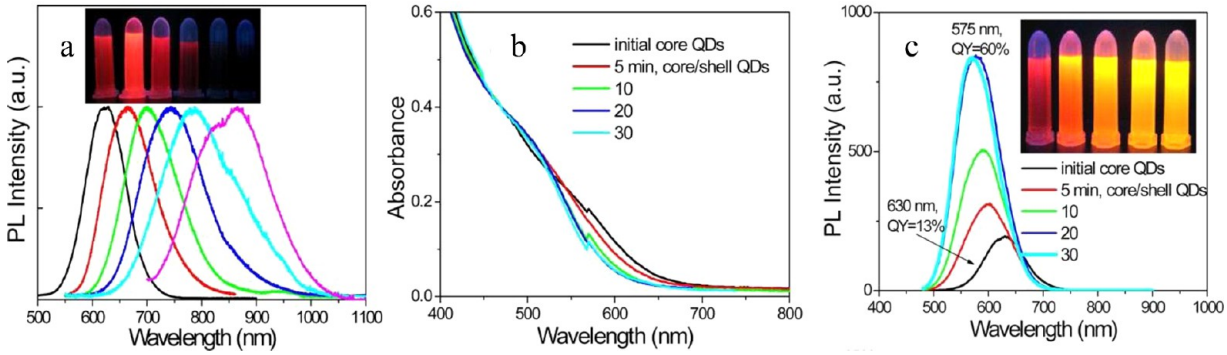

Figure 5. (a) PL spectra of CIS nanocrystals together with a digital photograph of the samples taken under a UV lamp. (b) Absorption and (c) PL spectra taken during the growth of a ZnS shell. The inset in c shows a photograph of the samples under UV lamp. Adapted with permission from ref 85. Copyright 2012 American Chemical Society.

easily tuned in the whole visible range. In alloyed structures with other cations the amount of internal defects (usually copper vacancies) is reduced, compared to pure CIS. Thus, frequently an increase of the PL quantum yield can be observed. Another advantage of this alloying strategy lies in the possibility to separate the control of the optical properties from the size and shape control. Especially, obtaining particles with a large bandgap by reducing their size is problematic and frequently cannot be achieved without suffering losses in the stability and the PL quantum yield, because of the large surface and the increased amount of surface defects.

Pan et al.[32] studied the structural and optical properties of ZnS-CIS alloys with cubic and hexagonal crystallographic structure (see Figure 6). The dependence of the bandgap from

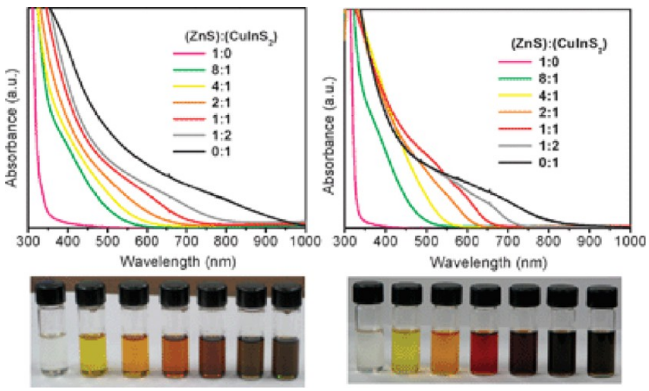

Figure 6. Absorption spectra and digital photographs of zincblende (left) and wurtzite (right) CIS-ZnS particles with different ZnS contents. Reproduced with permission from ref 32. Copyright 2009 The Royal Society of Chemistry.

the composition of the alloy can be described with the following equation

$$E_g(x) = xE_g^{CIS} + (1 - x)E_g^{ZnS} + bx(1 - x) \quad (5)$$

E_g^{CIS} and E_g^{ZnS} are the bulk bandgaps of CIS and ZnS, respectively, x is the molar fraction of CIS in the alloy, and b is the bandgap bowing parameter, which has to be introduced, because of the nonlinear dependence of the bandgap from the composition. The bowing parameter for both wurtzite and zinc blende CIS nanoparticles is strongly composition dependent and has larger values for ZnS-rich particles (see Figure 7). Thus, the optical properties of ZnS nanocrystals can be strongly influenced by alloying them with a small fraction of CIS.

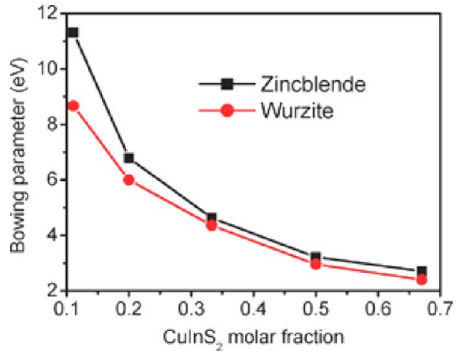

Figure 7. Bowing function of zincblende and wurtzite CIS-ZnS. Reproduced with permission from ref 32. Copyright 2009 The Royal Society of Chemistry.

2. Synthesis of CIS Nanocrystals. A general challenge in the synthesis of CIS nanoparticles arises from the fact, that the two cations of this ternary semiconductor have different chemical properties. In^{3+} is a hard Lewis acid, while Cu^{+} is a soft one; therefore, they differ in their reactivity towards sulfur compounds (normally, soft Lewis bases). And if the reactivity of both cationic precursors is not balanced, the formation of copper sulfides can be observed, instead of the growth of CIS nanocrystals. Simultaneous adjusting the reactivity of copper and indium monomers can be achieved by applying more than one kind of stabilizer, e.g., a thiol and a carboxylic acid, for regulating the activity of copper and indium monomers, respectively.[23] Also a high excess of only one stabilizer, e.g., in reactions using a thiol as solvent and ligand,[33] is a suitable way to reduce the reactivity of both cations to a similar level. Another strategy to circumvent the problem of different reactivities is the use of precursors containing both cations in one compound, the decomposition of this single molecular precursor sets free the same amount of copper and indium simultaneously, which promotes the formation of CIS, instead of a binary compound.[24,29,34,35]

CIS nanocrystals can be synthesized using a variety of metal salts and sulfur sources. Most of the syntheses are conducted in organic solvents, only a few water-based procedures have been described.[36−41] Best size and shape control could be obtained in hot-injection or heating-up procedures (see examples in Figures 8, 10, and 11). For an overview of the parameters of the

synthesis and the properties of the resulting particles, see Table 1.

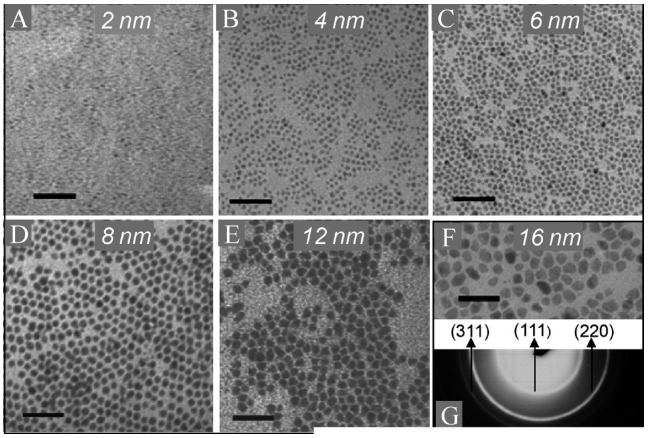

Figure 8. (a–f) TEM images of CIS nanocrystals of different sizes between 2 and 16 nm and (g) an electron diffraction pattern of the particles. The scale is 50 nm. Adapted with permission from ref 23. Copyright 2009 American Chemical Society.

2.1. Controlling the Crystallographic Structure. At room temperature, bulk CIS crystallizes in the chalcopyrite structure, in which copper and indium atoms are ordered within the unit cell. At elevated temperatures, a random distribution of the cations becomes thermodynamically more favored, which results in the formation of zincblende structure above 980 °C and wurtzite between 1045 and 1090 °C (melting point of CIS).[93] This cation disordered polymorphs have the advantage of more flexible stoichiometry (compared to the chalcopyrite structure), because both cations occupying the same lattice site can easily be exchanged for each other. Therefore, the Fermi energy of these materials can be tuned in a wide range, which makes them interesting, for example, for application in solar energy conversion. In contrast to the bulk material, nanocrystalline CIS can exhibit all three crystallographic structures at room temperature. Although the wurtzite structure of the nanoparticles can be unambiguously assigned based on their x-ray diffraction pattern, the zincblende and the chalcopyrite structure cannot always be distinguished from one another, especially if the reflections are broadened because of the small sizes of the crystallites. The lattice parameters of both structures are related to each other, $c_{CP} = 2c_{ZB}$, and the only structural difference is the ordering of the cations. This gives rise to several additional reflections in the chalcopyrite diffraction pattern, compared to the zincblende structure, which have low intensities. Thus, a clear assignment of the crystallographic structure is not always possible.

The first report about the synthesis of CIS nanoparticles with zincblende and wurtzite structure was published 2008 by Pan et. al,[51] who used copper and indium diethyl dithiocarbamate in octadecene (ODE), with oleylamine (OLAM) as activation agent and oleic acid (OA) or 1-dodecanethiol (1-DDT) as ligands, to obtain zincblende and wurtzite structure, respectively. By varying the ratio between the cationic precursors, the stoichiometry of the zincblende particles could be controlled in the range between $Cu_3InS_{3.1}$ and $CuIn_{2.2}S_{3.8}$. The size of the nanocrystals was adjusted between ~3 and ~30 nm by changing the temperature and the amount of oleylamine.

Norako et al.[59] synthesized CIS particles with wurtzite structure in a reaction with $In(acac)_3$ and CuCl in oleylamine, with 1-dodecanethiol as stabilizer, using di-tert-butyl disulfide as the sulfur source. They attribute the formation of the wurtzite phase to the coordination of oleylamine to the metal cation precursors and to the relatively slow release of the sulfur by di-tert-butyl disulfide.

Nose et al.[60] studied the formation of chalcopyrite and wurtzite CIS nanoparticles in reactions of CuI and $InCl_3$ in ODE, with trioctylphosphite (TOOP) as stabilizer. Elemental sulfur dissolved in triphenylphosphite (TPOP) was the source of sulfur. The crystallographic structure of the resulting particles was controlled by the addition of oleylamine or hexadecylamine (HDA). When the starting solution was stirred for 3 h at room temperature, prior to heating it to induce the formation of CIS nanocrystals, particles with wurtzite structure were generated. Whereas, freshly prepared solutions with an amine, or reaction, without addition of OLAM or HDA resulted in the growth of chalcopyrite particles. The authors observed different nucleation and growth rates in the two types of reactions. IR measurements revealed that when chalcopyrite particles were formed, the precursors in this reaction were relatively reactive CuI-TOOP, $InCl_3$-TOOP and S-TPOP complexes. Thus, the nucleation was fast, and the growth process relatively slow, which induced the formation of the thermodynamically stable chalcopyrite modification of the nanoparticles. The nucleation of wurtzite particles was slower and a smaller amount of particles was formed, because they originated from a reaction between more stable CuI-OLAM, $InCl_3$-OLAM, and S-TPOP complexes. Therefore, a higher concentration of monomers was available for the growth of the nanoparticles, which occurred faster than in the case of chalcopyrite particles. This resulted in the formation of the kinetically stable wurtzite phase.

Batabyal et al.[35] controlled the phase of CIS nanoparticles by changing the reaction temperature of the decomposition of a single source precursor ($(Ph_3P)CuIn(SC\{O\}Ph)_4$) in the presence of 1-DDT or TOPO. Zincblende nanoparticles were obtained, when the synthesis was conducted at 350°C, at lower temperatures and high TOPO concentration, wurtzite structure was obtained. In contrast to these results, Kruszynska et al.[74] reported the formation of zincblende particles in reactions of CuOAc and $InOAc_3$ with sulfur in OLAM at lower temperatures, while higher temperatures or the presence of thiols favored the formation of the wurtzite phase.

Chang and Waclawik[90] controlled the crystallographic structure of CIS nanocrystals by the coordination properties of the solvents and the reaction temperature. The crystalline $CuIn(SR)_x$ complex, which formed in coordinating solvent (OLAM), or at low temperature, led to the formation of wurtzite particles, while the generation of zincblende particles was observed in reactions with a $CuIn(SR)_x$ intermediate with lower crystallinity. The authors successfully applied this phase control strategy also in the synthesis of two other materials, Cu_2SnS_3 and Cu_2ZnSnS_4.

The structure of CIS nanocrystals synthesized with solvothermal methods can also been controlled by the choice of solvent. Huang et al.[87] obtained zincblende particles in reactions of $CuCl_2$, $InCl_3{\cdot}xH_2O$ and thioacetamide in OLAM, whereas nanocrystals with wurtzite structure formed when ethylenediamine was used as solvent. The authors assume the phase control is due to the different degrees of coordinating interactions of both solvents with the cations.

Table 1. Overview of the Experimental Procedures for the Synthesis of CIS Nanocrystals[a]

precursors, ligands, solvents	method/conditions	size, shape, structure	ref
$CuP(OPh)_3$, $In(P(OPh)_3)_3$, bis(trimethylsilyl)sulfide, acetonitril	RT, 1 day, slow injection	3.5 nm, quasi-spherical, CP	Czekalius et al. 1999[42]
Cu, In, S, ethylendiamine	280 °C, 6 h, solvothermal	20 × 800 nm, nanorods, CP	Jiang et al. 2000[43]
CuCl, In, S, water or benzene	200 °C, 12 h, solvothermal	15 nm, CP	Lu et al. 2000[44]
$Cu(S_2CNEt_2)$, $Cu(S_2CNEt_2)_2$, ethylenediamine	190 °C, 8 h, solvothermal	3−20 × 80−450 nm, nanorods, CP	Cui et al. 2001[45]
$(Ph_3)_2CuIn(SEt)_4$, dioctylphthalate	250 or 300 °C, 1 h, heat-up	500 nm, aggregates, CP	Castro et al. 2003[34]
$(Ph_3)_2CuIn(SEt)_4$, hexanethiol, dioctylphthalate	200 °C, 8 h, heat-up	2−4 nm, CP	Castro et al. 2004[24]
$Cu(S_2COEt)$, $In(S_2COEt)_3$, EG	196 °C, 15 min to 4 h, heat-up	3.6−38 nm, quasi-spherical, CP	Dutta et al. 2006[46]
$(TOP)_2CuIn(S(n\text{-}Pr)$ or $(t\text{-}Bu))_4$, DOP, benzene, toluene or hexane	2−218 h, photolysis	2 nm, CP	Nairn et al. 2006[29]
CuI, InI_3, S, OLAM, TOP, ODE	160−180 °C, 60−300 s, fast heating-up	3−6 nm, CP	Nakamura et al. 2006[47]
$Cu(OAc)_2$, $InCl_3$, CS_2, HDA, anisole	200 °C, 12 h, solvothermal	13−17 nm, polyhedral, CP	Du et al. 2007[48]
$[P(i\text{-}But)_3]_2CuIn(SEt)_4$ or $(PPh_3)_2CuIn(SEt)_4$, hexanethiol, dioctyl phthalate	140−170 °C, 20−30 min, microwave irradiation	3−5 nm, quasi-spherical, CP	Gardner et al. 2007[49]
$Cu(OAc)_2$, $In(OAc)_3$, 1-DDT, tri-n-octylamine	230 °C, heat-up	1.8−2.8 nm, quasi-spherical, CP	Kino et al. 2008[50]
$Cu(S_2CNEt_2)_2$, $In(S_2CNEt_2)_3$, OLAM, OA or 1-DDT, ODE	200 °C, 4 min, hot-injection	2−28 nm, quasi-spherical, ZB or WZ	Pan et al. 2008[51]
$Cu(acac)_2$, $In(acac)_3$, o-dichlorobenzene, S	180 °C, 1 h, hot-injection	8−12 nm, quasi-spherical, CP	Panthani et al. 2008[52]
CuI, InI_3, S, OLAM, TOP, ODE	160−240 °C, heat-up	4 nm, quasi-spherical, CP	Uehara et al. 2008[21]
CuCl, $In(NO_3)_3$, S, octadecylamine	120 °C, 10 min, heat-up	7 nm, quasi-spherical	Wang et al. 2008[53]
Cu(OAc), $In(NO_3)_3$, thioacetamide, CTAB, EG	80 °C, hot-injection, subsequent heating to 199 °C	80−100 nm, hollow spheres, CP	Zhang et al. 2008[54]
$Cu(OAc)_2$, $In(OAc)_3$, 1-DDT, ODE	240 °C, 2.5 h, heat-up	2−5 nm, quasi-spherical and rods, CP	Zhong et al. 2008[55]
$(Ph_3P)CuIn(SC\{O\}Ph)_4$, 1-DDT, TOPO	350 °C, heat-up	platelike, WZ 5−10, quasi-spherical, ZB	Batabyal et al. 2009[35]
$CuCl_2$, $InCl_3$, Na_2S, water, mercaptoacetic acid	90 °C, 30 min, microwave heating	3 nm, quasi-spherical, CP	Bensebaa eta al. 2009[36]
Cu-oleate, In-oleate, 1-DDT, OLAM	215−300 °C, 20 min, heat-up	nanorods, WZ	Connor et al. 2009[56]
CuI, $InCl_3$, acetonitril, hexamethyldisilathian, triphenylphosphite,	RT, 24 h, slow addition of hexamethyldisilathian	CP	Courtel et al. 2009[57]
CuCl, $InCl_3$, thiourea, OLAM	240 °C, 1 h, heat-up	13.4 × 5.7 nm, nanodiscs, CP/WZ	Koo et al. 2009[58]
CuI, $In(OAc)_3$, 1-DDT, ODE	200−270 °C, 15−290 min, heat-up	3 nm, quasi-spherical, CP	Li et al. 2009[28]
CuCl, $In(acac)_3$, di-tert-butyl disulfide, 1-DDT, OLAM	180 °C, 33 min, hot-injection	7 nm, quasi-spherical, WZ	Norako et al. 2009[59]
CuI, $InCl_3$, S/triphenylphosphite, trioctylphosphite (TOOP), HDA, ODE	heat-up, 200−240 °C, 2−10 min	5 nm, ZB, WZ	Nose et al. 2009[60]
$(Ph_3P)_2Cu(\mu\text{-}SEt)_2In(SEt)_2$, dioctyl phthalate or benzyl acetate, 1,2-ethandiol	100−200 °C, 30 min, microwave heating	1.8−10.8 nm, CP	Sun et al. 2009[61]
CuCl, $InCl_3$, thiourea, ethanolamine	180 °C, 24 h, solvothermal	nanoplates, hollow spheres, flowerlike spheres, WZ	Qi et al. 2009[62]
$Cu(OAc)_2$, $In(OAc)_3$, S, TOP, 1-DDT, OA, SA, ODE	180 °C, 5 min, hot-injection	2−20, quasi-spherical, ZB	Xie et al. 2009[23]
$Cu(OAc)_2$, $In(OAc)_3$, 1-DDT, t-DDT, TOPO, OLAM	240 °C, 30 s to 1 h, hot-injection	various sizes, nanorods, P-shaped, hexagonal plates, WZ	Kruszynska et al. 2010[63]
CuCl, $InCl_3$, S, OLAM, hexane	110−170 °C, 1 h, solvothermal	3−5 nm, CP	Li and Teng 2010[64]
$CuCl_2$, $InCl_3$, S, bis(N-hexyldithiocarbamate) zinc, OLAM, TOP, ODE	190 °C, 10 min, hot-injection	3 nm, ZB	Pons et al. 2010[65]
$Cu(acac)_2$, $In(acac)_3$, S, OLAM, o-dichlorobenzene	180 °C, 1 h, heat-up	20 × 200, nanotubes, CP	Shi et al. 2010[66]
$(Ph_3P)_2Cu(\mu SEt)_2In(SEt)_2$, ethanedithiol, benzyl acetate	160−240 °C, 1 h, microwave heating	2−4 nm, CP	Sun et al. 2010[67]
$Cu(NO_3)_2$, $In(OAc)_3$, S, 1-DDT, OA, ODE, OLAM	175 °C, 10−15 min, hot-injection	3−4 nm, WZ	Yong et al. 2010[68]
CuCl, $InCl_3$, Na_2S, 4-bromothiophenol, ethanol	200 °C, 16 h, solvothermal	2−4 nm, ZB	Yue et al. 2010[69]
CuI, $In(OAc)_3$, 1-DDT, OA, ODE	200 °C, 20−120 min, heat-up	3.5−7.5 nm, triangular, CP	Zhong et al. 2010[70]
CuCl, $InCl_3$, 1-DDT, OLAM, (ODE or OA)	290 °C, hot-injection	various sizes, pyramides, cones, bullet-shaped, WZ	Bao et al. 2011[71]
CuCl, $InCl_3$, S, OLAM	265 °C, 1.5 h, heat-up	15−17 nm, quasi-spherical, CP	Chiang et al. 2011[72]

Table 1. continued

precursors, ligands, solvents	method/conditions	size, shape, structure	ref
CuI, $InCl_3$, N-methylimidazole, Li_2S,	RT, 2 h	2.2−21.9 nm, quasi-spherical, CP	Courtel et al. 2010[73]
$Cu(OAc)_2$, $In(OAc)_3$, 1-DDT, t-DDT, S-OLAM, TOPO, OLAM	240 °C, 50 s to 1 h, hot-injection and heat-up	triangular pyramids, WZ and ZB	Kruszynska et al. 2010[74]
Cu(OAc), $In(OAc)_3$, S, OLAM,	200 °C, 2 h, hot-injection	25 nm, nanoflowers, CP	Luo et al. 2010[75]
CuI, $In(OAc)_3$, 1-DDT	230 °C, 5 min to 1 h, heat-up	3−8 nm, triangular, CP	Li et al. 2011[33]
$CuCl_2$, $InCl_3$, L-cysteine, ethylenediamine, water	200 °C, 18 h, solvothermal	300−500 nm, CP	Liu et al. 2011[76]
$Cu(NO_3)_2$, $In(NO_3)_3$, 1-DDT, OLAM, OA	240 °C, 30 min, heat-up	quasi-spherical, rods, WZ	Lu et al. 2011[77]
CuI, $In(OAc)_3$, 1-DDT, MA, ODE	180 °C, 5−6 h, solvothermal	3 nm, CP	Nam et al. 2011[78]
CuI, $In(OAc)_3$, 1-DDT, ODE	180 °C, 5−6 h, solvothermal	1.4−3.6 nm, CP	Nam et al. 2011[79]
CuI, $In(OAc)_3$, 1-DDT, MA, ODE	230 °C, 2 h, hot-injection	3 nm, CP	Park and Kim 2011[80]
CuI, $InCl_3$, S, OLAM	120−220 °C, 3−120 min, heat-up, microwave heating	2−4 nm and 5−10 nm, CP	Pein et al. 2011[81]
CuCl, $InCl_3$, thiourea, diethylene glycol	180 °C, 2 h, hot-injection	80−100 nm, hexagonal plates, WZ	Sheng et al. 2011[82]
$Cu(OAc)_2$, $In(OAc)_3$, 1-DDT, OA, TOP, ODE	120 °C, 10 min, heat-up	9−11.5 nm, cubic, CP	Tang et al. 2011[83]
$Cu(SON(CNPr_2)_2)_2$, $In(SON(CNPr_2)_2)_3$, OLAM, 1-DDT	200−280 °C, 1 h, heat-up	10 nm, tigonal, quasi-spherical, hexagonal, CP	Abdelhady et al. 2012[84]
CuI, $In(OAc)_3$, 1-DDT, OA, ODE	210 °C, 60 min, heat-up	5 nm, CP	Chen et al. 2012[22]
$Cu(OAc)_2$, $In(OAc)_3$, 1-DDT, OA, ODE	215−280 °C, heat-up	2.5 nm, ZB	Deng et al. 2012[85]
$Cu(OAc)_2$, $In(OAc)_3$, 1-DDT, $Sn(OAc)_2Cl_2$	200 °C, 120 min, heat-up	polygonal, CP	He et al. 2012[86]
$CuCl_2$, $InCl_3$, thioacetamide, OLAM or ethylenediamine	160 °C, 12 h, solvothermal	10−20 nm, ZB or WZ	Huang et al. 2012[87]
$CuCl_2$, $InCl_3$, thioacetamide, mercaptopropionic acid, water	150 °C, 21 h, solvothermal	2 nm, CP	Liu et al. 2012[38]
$Cu(acac)_2$, $In(acac)_3$, dodecylphosphonic acid, TOPO, hexadecylamine, bis(trimethylsilyl) sulfide	120 °C, 3 min, hot-injection	4.0−5.6 nm, quasi-spherical, CP	Niezgoda et al. 2012[27]
CuCl, $InCl_3$, poly(vinyl) pyrolidone or hexadecyl timethyl ammonium bromide, thiourea, diethylene glycol, EG	180 °C, hot-injection	100−200 nm, polyhedral 500 nm, flowerlike	Sheng et al. 2012[88]
CuI, $In(OAc)_3$, 1-DDT	230 °C, 5 min, heat-up	2 nm, CP	Song et al. 2012[89]
$CuSO_4$, $InCl_3$, bovine serum albumin, thioacetamid, water	RT, 24 h	<10 nm, irregular shape, CP	Wang et al. 2012[39]
CuI, $In(OAc)_3$, 1-DDT, ODE	220 °C, overnight, heat-up	9 nm, 25 nm triangular pyramid, ZB	Chang and Waclawik 2013[90]
CuI, $In(OAc)_3$, 1-DDT, OLAM	190 °C, overnight, heat-up	hexagonal nanodisc, WZ	
CuCl, $InCl_3$, Na_2S, sodium citrate, thiourea, L-glutathion, water	95 °C, 40 min, heat-up	2.1 nm, ZB	Chen et al. 2013[40]
Cu(OAc), $InCl_3$, mercaptoacetic acid, Na_2S, water	RT, 2 h	4 nm, quasi-spherical,CP	Luo et al. 2013[41]
$In(OAc)_3$, CuCl, 1-DDT, ODE	240 °C, 1 h, heat-up	∼7 nm, CP	Yao et al. 2013[91]
CuI, $In(OAc)_3$, 1-DDT, diphenylphosphine sulfide	50−160 °C, heat-up	2.8−3.4 nm, quasi-spherical, CP	Yu et al. 2013[92]

[a]acac, acetylacetonate; CP, chalcopyrite; 1-DDT, 1-dodecanethiol; t-DDT, tert-dodecanethiol; EG, ethylene glycol; HDA, hexadecylamine; MA, myristic acid; OA, oleic acid; OAc, acetate; ODE, octadecene; OLAM, oleylamine; SA, stearic acid; TOP, trioctylphosphine; TOPO, trioctylphosphine oxide; WZ, wurtzite; ZB, zincblende.

The formation of CIS nanocrystals with wurtzite structure can, furthermore, been observed, if the growth of CIS goes through a copper sulfide intermediate.[56,63,77,94] Hexagonal Cu_2S and wurtzite CIS have nearly the same anion lattice (see Figure 9), thus, copper sulfide can play the role of a template for the growth of CIS with wurtzite structure. As will be discussed in the next section, it can also play an important role in the shape control of CIS nanocrystals.

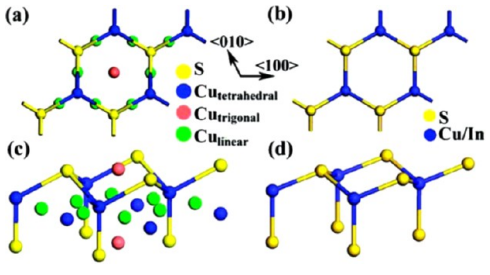

Figure 9. Crystallographic structures of (a, c) hexagonal copper sulfide and (b, d) CIS. Reprinted with permission from ref 56. Copyright 2009 American Chemical Society.

2.2. Shape Control. The final shape of the nanocrystals obtained in colloidal synthesis results from a delicate interplay of many factors, including the reaction kinetics (e.g., the rate of the transport of the monomers to the surface) and the thermodynamic stability of particular phases or the surface energy of the facets terminating the crystallite. All these factors can be to a large extent adjusted by the choice of the parameters of the synthesis, such as the kind and the concentration of the starting materials, ligands and solvents, the reaction temperature and time. The multitude of possible combinations of these parameters together with the extensive research activities in the area of colloidal synthesis of nanocrystalline materials led to the development of synthetic procedures for a variety of uniform semiconductor and metal particles with different shapes, ranging from faceted 0D nanocrystals, through 1D nanorods and nanowires, to 2D nanoplates or extended thin nanosheets, and some more exotic shapes, such as arrows, stars or rings. Compared with, for

example, II–VI semiconductors, the shape control of CIS nanocrystals is less advanced at the present stage and still requires a lot of optimization and thorough investigations of the underlying reaction mechanisms. This is partly due to the fact that new growth pathways were found in the synthesis of CIS nanocrystals, which are specific for multinary materials, i.e., the formation of binary intermediates and hybrid structures, which allow for new ways of shape control. Especially the formation of copper sulfide, which can frequently been observed in reactions of copper, indium and sulfur compounds,[23,63] can be an effective way of controlling the shape of CIS nanoparticles.[63] Copper sulfide forms several non-stoichiometric, copper deficient phases, which exhibit high cation mobility already at moderate temperatures; the copper ions move like a fluid throughout the cation sites. This facilitates the exchange with In^{3+} ions that have the same radius as Cu^{+}. Furthermore, wurtzite CIS and copper sulfide share the same anion lattice (Figure 9). Therefore, the formation of copper sulfide-CIS hybrid nanostructures or a phase transformation from copper sulfide to CIS requires little lattice distortion and is promoted by the high cation mobility.

The first synthesis of CIS nanorods, which involved copper sulfide intermediates was described by Connor et al.,[56] who obtained wurtzite particles with length up to ca. 110 nm and irregular thickness in the size range of 10-50 nm (Figure 10).

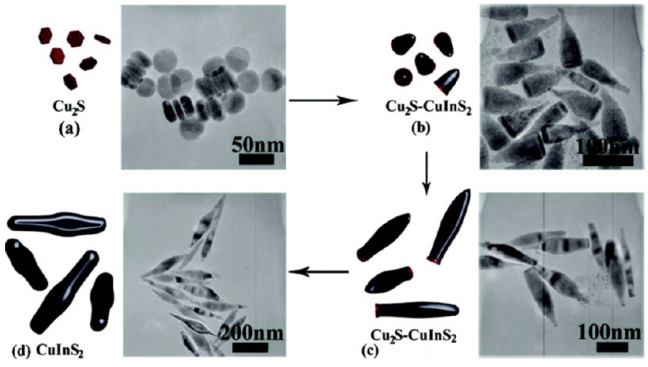

Figure 10. (d) The formation of wurtzite CIS nanorods, (a) starting with Cu_2S nanoplates as seeds and (b, c) going through Cu_2S-CIS hybrid structures as intermediates. Reprinted with permission from ref 56. Copyright 2009 American Chemical Society.

The synthesis starts with the formation of Cu_2S (chalcocite) nanodiscs; then, CIS nanoparticles start growing on one side of them. The nanodiscs maintain their thickness throughout the growth process of CIS nanorods within the biphasic structure, until they, finally, are also converted to CIS. This process is assumed to be a solid–solid seed-based phase transition, and takes place abruptly about 20 minutes after the nucleation of the copper sulfide seeds. The authors explain the formation of CIS nanocrystals on one side of the copper sulfide nanoplates, and the one-dimensional growth of CIS nanorods with the different reactivity of (001) faces of wurtzite structure, among which one is sulfur-terminated, the other one is covered with copper and indium ions.

A higher degree of shape control was obtained by Kruszynska et al.,[63] who synthesized various shapes of CIS nanocrystals based on the formation of $Cu_{2-x}S$-CIS hybrid structures (Figure 11). Nanorods, dimeric rods, hexagonal plates and p-shaped particles were obtained by changing the size and the position of the copper sulfide part of the hybrid structure. In

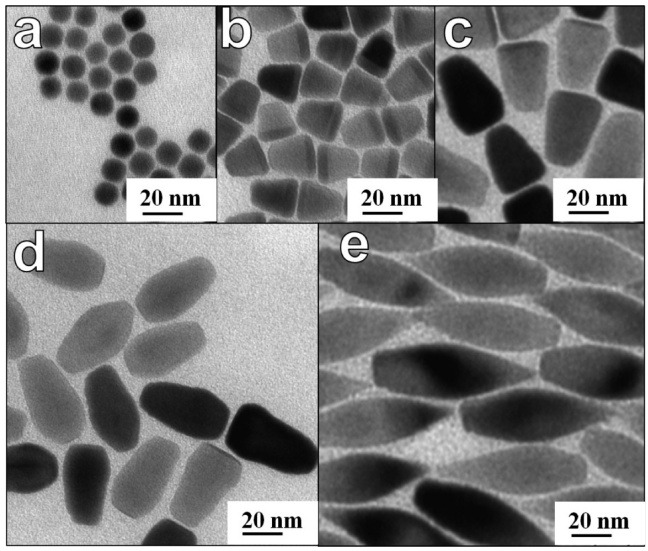

Figure 11. Growth process of CIS nanocrystals starting with (a) the formation of spherical $Cu_{2-x}S$ particles going through (b–d) CIS-$Cu_{2-x}S$ intermediates before (e) the formation of pure CIS. Reprinted with permission from ref 63. Copyright 2010 American Chemical Society.

contrast to the mechanism suggested by Connor et al.,[56] where the nucleation of CIS takes place on one side of the copper sulfide nanoplate, in the work by Kruszynska et al.[63] the reaction starts with the formation of quasi-spherical copper sulfide particles and the growth of CIS seeds can be observed inside these particles. After the CIS seeds have reached a certain size, a hybrid structure is formed, which consists of two discs, composed of CIS and coppers sulfide, connected together. The further growth of the CIS-phase takes place solely at the interface of the two phases of the hybrid nanoparticles. At later stages of the synthesis the copper sulfide phase gradually disappears and pure CIS nanocrystals are formed.

Another work about the formation of anisotropic shapes of CIS nanocrystals was reported by Lu et al.[77] Heterostructured nanoparticles (CIS-copper sulfide), waterdrop-like, spindle-like, and straight nanorods were synthesized by changing the surfactants and the ratio between the starting materials. Also in this study the formation of copper sulfide particles is assumed to be the first step of the synthesis.

CIS nanoribbons with wurtzite structure, length of 2–3 μm and width of 20–50 nm were synthesized using $Cu_{1.75}S$ nanoparticles as catalyst (Figure 12).[95] The formation of nanoribbons with rectangular cross-section was explained based on a structural analysis of the grain boundary between $Cu_{1.75}S$ and CIS, which is composed of (0160) planes of $Cu_{1.75}S$ and (110) planes of CIS. The lattice mismatch along the $(1\bar{1}0)$‖$(\bar{1}\bar{6}00)$ direction is relatively small (0.67%), which allows for the formation of ribbons with a width of 20–50 nm. In contrast, the lattice mismatch along the (002)‖(004) direction is 3.82%; therefore, epitaxial growth in this direction is limited, which results in a thickness of 15 nm.

It is not only copper sulfide that can be applied as a catalyst in the synthesis of CIS nanostructures. Ag_2S, which is, similarly to $Cu_{2-x}S$, a material with high cation mobility, can also promote the formation of elongated CIS nanocrystals. Li et al.[96] demonstrated the formation of nanowires with length of 1–2 μm and diameter of 20–50 nm (Figure 13). In contrast to the synthesis using $Cu_{1.75}S$ nanoparticles as catalyst,[95] the lattice

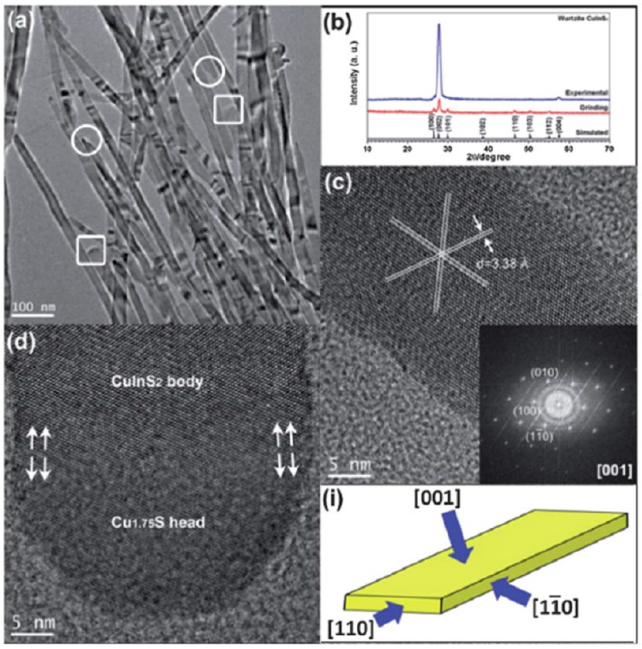

Figure 12. (a, c, d) TEM images and (b) XRD pattern of CIS nanoribbons. (i) The schematic morphology of the nanoribbon with the crystallographic orientation. Reproduced with permission from ref 90. Copyright 2013 The Royal Society of Chemistry.

mismatch between Ag_2S and CIS is almost the same along the two growth directions perpendicular to the length of the nanowire, and thus wires, instead of ribbons, are formed with Ag_2S as catalyst.

2.3. Alloys and Core–Shell Structures Based on CIS Nanocrystals. Synthetic procedures for the synthesis of pure CIS can be further modified to obtain CIS-alloys with ZnS,[32,63,83,97−102] CdS,[103] $CuGaS_2$,[104,105] and Cu_2SnS_3.[37] In most cases the alloys are formed, when additional cations (Zn^{2+}, Cd^{2+}, Ga^{2+}, or Sn^{2+}) are present in the reaction solution. Also a two-step strategy can be applied to obtain alloyed particles: a reaction of preformed CIS particles with Zn compounds (usually zinc stearate) leads to an exchange of some fraction of the indium and copper cations at elevated temperatures (210°C).[30,83,106] For an overview of the synthetic procedures for alloyed materials based on CIS nanocrystals, see Table 2.

Several procedures have been developed to cover a CIS core with a ZnS shell.[23,28,33,65,78,80,85,107−109] The zinc precursor (zinc acetate, stearate, or ethylxanthate) can be added to the solution of as synthesized CIS nanocrystals, without an additional purification step, and a ZnS shell forms, when this mixture is heated to temperatures above 210 °C for 30 min to 2 h.[80,85,110] The unpurified CIS solution can still contain enough sulfur precursor, so that the addition of sulfur is not always necessary.[80,85]

Coating CIS or CIS-ZnS particles with a ZnS shell shows a beneficial effect on the photoluminescence properties of the cores. However, in most cases, a blue-shift of the absorption and the emission band can be observed (Figure 14), indicating changes in the size or composition of the CIS core. This behavior is different from most other type I core–shell structures, in which a red-shift of the absorption and emission follows the formation of the shell, because of a slight delocalization of the charge carriers into the shell material. Several different explanations for the blue shift observed in CIS-ZnS core-shell particles have been suggested, including surface reconstruction,[28] the inter-diffusion of Zn atoms,[65] or etching of the core material;[33] however, these assumptions were not verified by further experimental evidence. Park and Kim[80] studied the formation of CIS-ZnS core–shell structures with different zinc precursors and found cation exchange in the outer layer of the CIS nanocrystals (Figure 15) to be the explanation for the change of the optical properties (large blue-shift of both the absorption and the emission, see Figure 14).

2.4. Surface Characterization and Functionalization. A variety of surfactants can be applied in the synthesis of CIS nanoparticles, e.g., amines, thiols, carboxylic acids, phospines or phosphonic acids. As shown before (see Table 1), a mixture of different surfactants is frequently applied in the synthesis of CIS, therefore, the surface of CIS nanocrystals might be covered by a ligand shell composed of several different molecules.

Zhong et al.[70] conducted the synthesis of CIS nanoparticles in presence of both DDT and OA; however, they did not observe a CO band in the IR spectrum of the particles. Thus, in spite of the presence of oleic acid in the reaction solution, this ligand was not present on the surface of the particles. This can be rationalized when taking into account the composition of the particles synthesized within this study, which were copper rich, starting with Cu/In ratio of 2.4:1 (reaction time: 20 min) and ending with 1.15:1 (120 min)). According to the hard and soft acids and bases theory thiols (soft bases) form stronger bonds with copper ions (soft acids), than carboxylic acids (hard bases). Thus, copper rich particles can be more efficiently stabilized by DDT than by OA.

All surfactants applied in the colloidal synthesis of CIS nanocrystals have a functional group with an electron pair that can bind to metal atoms on the surface of CIS nanoparticles and one or more relatively long carbon chains, which form a dense hydrophobic shell, providing colloidal stability in unpolar solvents. In most cases these ligands, which are appropriate for size and shape control are of limited suitability for further applications of nanoparticles.[111] If the particles are supposed to be applied in aqueous medium (e.g., for biomedical applications) a ligand exchange or a modification of the ligand shell has to be carried out.[85,92,109,112,113] But not only required solubility in specific solvents is a motivation for ligand exchange. Also the thickness of the ligand shell might prevent efficient application of nanocrystalline materials; especially, if charge transport between the particles is involved, the influence of an insulating ligand shell has to be reduced.[111] The complete removal of the original ligand shell turns out to be difficult, furthermore, the unprotected particles exhibit surface defects, which serve as traps for charge carriers. Thus, a ligand exchange with small organic or inorganic molecules, which prevent aggregation and reduce the amount of surface defects, while enabling charge transport, turns out to be a more efficient way of surface modification in view of further applications.

Effective ligand exchange can be achieved with thiols such as mercaptopropionic acid, if the original ligand shell is composed of fatty acids or amines.[64,107,114−116] However, no exchange with mono-thiol group ligands can be achieved, if the original particles are already stabilized by thiols, such as DDT.[23,101] In this case dihydrolipoic acid, which possesses two thiol anchoring groups, can be used to modify the surface and to render the particles water-soluble.[28,92,101] Phase transfer into water can also be achieved without ligand exchange, by non-

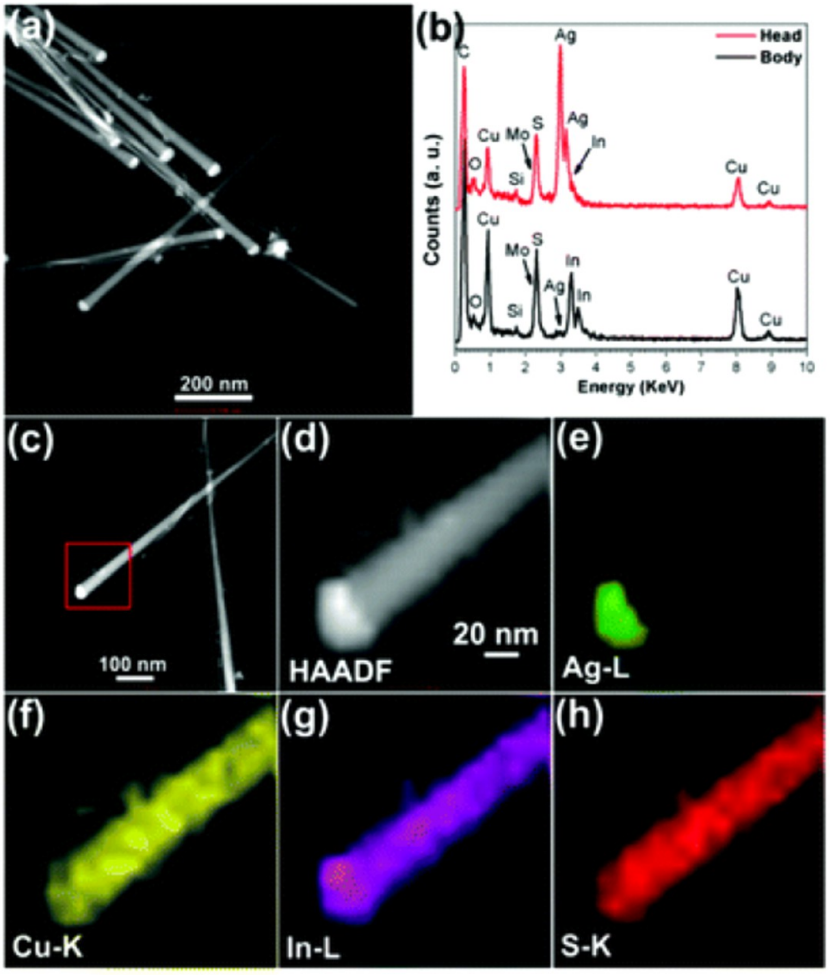

Figure 13. HAADF–STEM images of CIS nanowires. (a) STEM image, (b) EDS spectra collected from head and body part of nanowires. Si and Mo element peaks attributed to EDS detector and molybdenum grid, (c) STEM image, (d) HAADF image, (e–h) STEM–EDS elemental maps of CIS nanowire with Ag_2S as catalyst, Ag, Cu, In, and S, respectively. Reproduced with permission from ref 91. Copyright 2013 The Royal Society of Chemistry.

covalent interaction of the original ligand shell with other molecules such as (1-tetradecyl) trimethylammonium bromide (TTAB,)[110] or poly(ethylene glycol) methacrylate (PEGMA),[114] which possess both hydrophobic groups, which can intercalate the hydrophobic ligands, and hydrophilic parts, which provide water solubility.

In the last few years, the application of all inorganic ligands, such as metal chalcogenides or small metal-free anions, have attracted increased attention,[117,118] because they are able to stabilize inorganic nanocrystals efficiently in polar solvents without forming an insulating layer on the surface of the nanocrystals; thus, the charge transport and the application of the nanocrystals in devices is facilitated. Ligand exchange with such inorganic ligands was demonstrated for many different materials and can also be applied to CIS nanoparticles. Yao et al.[91] studied the ligand exchange, starting with 1-DDT-capped particles (Figure 16); they confirmed successful surface modification with S^{2-} ions using FTIR absorption spectroscopy, which showed no hydrocarbon related bands in the sample treated with S^{2-} ions. The thermogravimetric analysis showed a much lower weight loss after ligand exchange, because of the absence of the bulky organic ligands. TEM and XRD (Figure 16b) measurements revealed a slight reduction of the size of the particles after the ligand exchange procedure.

3. Application of CIS Nanocrystals. *3.1. Biomedical Applications.* Semiconductor nanocrystals as fluorescent probes for bioimaging offer several advantages compared to organic dyes: nanoparticles are more stable under light irradiation, they have narrow emission bands, which can be easily tuned by the size and the composition of the crystallites and the broadband absorption enables excitation of several probes with a single wavelength. CIS or CIS-ZnS nanocrystals have also the advantage of being a low toxic material, which makes them suitable candidates not only for in vitro but also in vivo studies. Another advantage of CIS is the relatively long fluorescence decay time in the order of magnitude of several hundreds of nanoseconds, which is typical for defect related emission. When using CIS nanoparticles in biolaballing, long delay times between photoexcitation and detection reduce the background signals from the biological sample, which have decay times up to 10 ns.[28]

First in vivo observations of the distribution of CIS-ZnS nanocrystals tranfered into water by ligand exchange with lipoproic acid in a mouse were conducted 2009 by Li et al.[28] Later, several studies showed the applicability of bioconjugated CIS-ZnS nanocrystals in imaging of e.g. tumor cells (see example in Figure 17).[28,65,68,85,92,109,113,114,119] Also, a two-photon absorption was observed in CIS-ZnS nanocrystals,[83]

Table 2. Overview of the Experimental Procedures for the Synthesis of CIS-Based Alloy Nanocrystals[a]

precursors, ligands, solvents	method/conditions	size, shape, structure, photoluminescence quantum yield (PLQY)	ref
	CIS-ZnS Alloy		
$Cu(dedc)_2$, $In(dedc)_3$, $Zn(dedc)_2$, ODE, OLAM, OA or 1-DDT	2 min, 200 °C, hot injection	quasi-spherical, zinc blend and wurtzite	D. Pan 2009[32]
$Cu(OAc)_2$, $In(OAc)_3$, $Zn(OAc)_2$, OLAM, TOPO, 1-DDT, t-DDT	5 min, 240 °C, hot injection	nanorods, wurtzite	M. Kruszynska 2010[63]
CuOAc, $In(OAc)_3$, zinc stearate, zinc ethylxanthate, 1-DDT, ODE	240 °C, slow precursor injection via syringe pump	Cu_2S-(CIS-ZnS alloy) heterostructure nanorods, wurtzite	J.-Y. Chang 2011[99]
$Cu(OAc)_2$, $In(OAc)_3$, $Zn(OAc)_2$, ODE, S-OLAM	15 min, 150–240 °C, hot injection	quasi-spherical, zinc blend, 70% PLQY	J. Zhang 2011[100]
$Cu(OAc)_2$, $In(OAc)_3$, $Zn(OAc)_2$, 1-DDT, ODE, S-ODE	5 min to 2 h, 230 °C, hot injection	quasi-spherical, zinc blend, 3% PLQY	W. Zhang 2011[97]
$Cu(OAc)_2$, $In(OAc)_3$, $Zn(OAc)_2$, 1-DDT, OA, ODE, S-ODE	hot injection	quasi spherical, zinc blend, 40% PLQY	J. Feng 2011[101]
CuOAc, $In(OAc)_3$, zinc stearate, 1-DDT, ODE	two-step method: reaction of CIS seeds with a zinc precursor	10.5 nm, cubic, zinc blend, 39% PLQY	X. Tang 2011[83]
CuI, $In(OAc)_3$, $(Zn(S_2CNEt_2)_2$, 1-DDT, OA, OLAM, ODE	30 min, 180 °C, hot injection of OLAM	quasi spherical, zinc blend, 10% PLQY	H.-J. Pan 2012[108]
$Cu(dedc)_2$, $In(dedc)_3$, $Zn(dedc)_2$, 1-DDT, OA, ODE,	60 min, 250 °C, heat-up	nanorods, wurtzite	C. Ye 2012[98]
CuCl, $InCl_3$, OLAM, $Zn(dedc)_2$, TOP, ODE	155 °C, heat-up	3.5 nm, quasi-spherical	N. Guijarro 2012[102]
CuI, $In(OAc)_3$ 1-DDT, zinc stearate	two-step method: reaction of CIS seeds with a zinc precursor	2–3 nm, chalcopyrite, 80% PLQY	Trizio 2012[30]
CuI, $In(OAc)_3$ 1-DDT, zinc stearate, OA, ODE	70 min, 210–290 °C, heat-up	3–6 nm, tetrahedral, zinc blend, 5% PLQY	W. Guo 2013[109]
	CIS-CdS-ZnS Alloy		
$Cu(dedc)_2$, $In(dedc)_3$, $Zn(dedc)_2$, $Cd(dedc)_2$, OLAM, OA, toluene	90 min, 180 °C, solvothermal	9 nm, zinc blend	X. Wang 2010[103]
	CIS- Cu_2SnS_3 Alloy		
CuCl, $SnCl_2$, $InCl_3$, OLAM, S-OLAM	60 min, 200–240 °C, hot injection	quasi-spherical, zinc blend	Q. Liu 2011[37]
	CIS-$CuGaS_2$ Alloy		
CuI, $In(OAc)_3$, $Ga(acac)_3$, 1-DDT	5 min, 230 °C, heat-up	quasi-spherical, zinc blend	W.-S. Song 2012[104]
$Cu(acac)_2$, $In(acac)_3$, $Ga(acac)_3$, 1-DDT, t-DDT, TOPO, OLAM, ODE	hot injection	35 nm, bulletlike, WZ	Wang 2011[105]

[a]acac, acetylacetonate; dedc, diethyldithiocarbamate; 1-DDT, 1-dodecanethiol; t-DDT, tert-dodecanethiol; EG, ethylene glycol; HDA, hexadecylamine; MA, myristic acid; OA, oleic acid; OAc, acetate; ODE, octadecene; OLAM, oleylamine; SA, stearic acid; TOP, trioctylphosphine; TOPO, trioctylphosphine oxide.

which is particularly interesting for bioimaging: it enables the excitation of CIS-ZnS nanoparticles with wavelengths lying in the near infrared, a spectral range without a strong absorption from water and biological tissue. CIS-ZnS nanocrystals were also combined with a Gd(III) complex, to obtain a biocompatible magnetic resonance/optical nanoprobe.[119]

3.2. Photocatalysis. In photocatalysis, electron-hole pairs generated by light irradiation are used to initiate chemical reactions. TiO_2 is an extensively studied photocatalyst, because of its high activity and stability, and low cost and toxicity. However, a drawback of TiO_2 is its large bandgap, and consequently, the necessity to excite it with UV light. Therefore, much effort has been put into development of visible-light driven photocatalysts, which more efficiently use the solar irradiation. It turned out that a combination of TiO_2 and CIS (or ZnS-CIS) nanocrystals can be an effective photocatalyst absorbing visible light. The relative positions of the energy levels of both materials enable charge separation; the photogenerated electrons are transferred from CIS to TiO_2, whereas the holes remain in the CIS nanocrystals (see Figure 18). The combination of CIS or CIS-ZnS and TiO_2 was successfully used in the process of degradation of organic pollutants,[98,120,121] whereas CIS and CIS-ZnS alone were shown to be a suitable photocatalyst for the sunlight-driven H_2 evolution.[122,123]

3.3. Solar Energy Conversion. The efficiency of solar cells based on $Cu(In,Ga)(S,Se)_2$ reached 20%, which is a record value among thin film devices.[124] Unfortunately, their fabrication requires high production and investment costs, which hinders their widespread application and pushes forwards efforts to find low-cost alternative methods to create thin-film devices. One of them is the use of nanocrystals inks.[52,88,125] Solar cells fabricated with $Cu(In,Ga)(S,Se)_2$ nanocrystals inks show promising results (~4.5% efficiency), however they do not reach the performance of photovoltaic devices produced with standard vacuum and high temperature techniques. CIS nanoparticles films, sintered at 400°C and subjected to selenization process, exhibit an even lower power conversion efficiency of ~0.74%.[87] Better results (4% efficiency) than with colloidal nanocrystals were obtained when a CIS nanoparticle film was formed in situ.[126]

Compared with thin-film solar cells, devices based on conductive polymers offer several advantages: they can be fabricated from solution, and thus with low cost methods, and if needed, on flexible substrates. An efficiency of 8.4% was reached in a single junction low-bandgap polymer cell.[127] Combining organic and inorganic material in an active layer of a solar cell is expected to improve the performance of polymer based devices even further, because of the possibility to improve the absorption properties of the active layer and the electron transport through the device. However, in spite of the

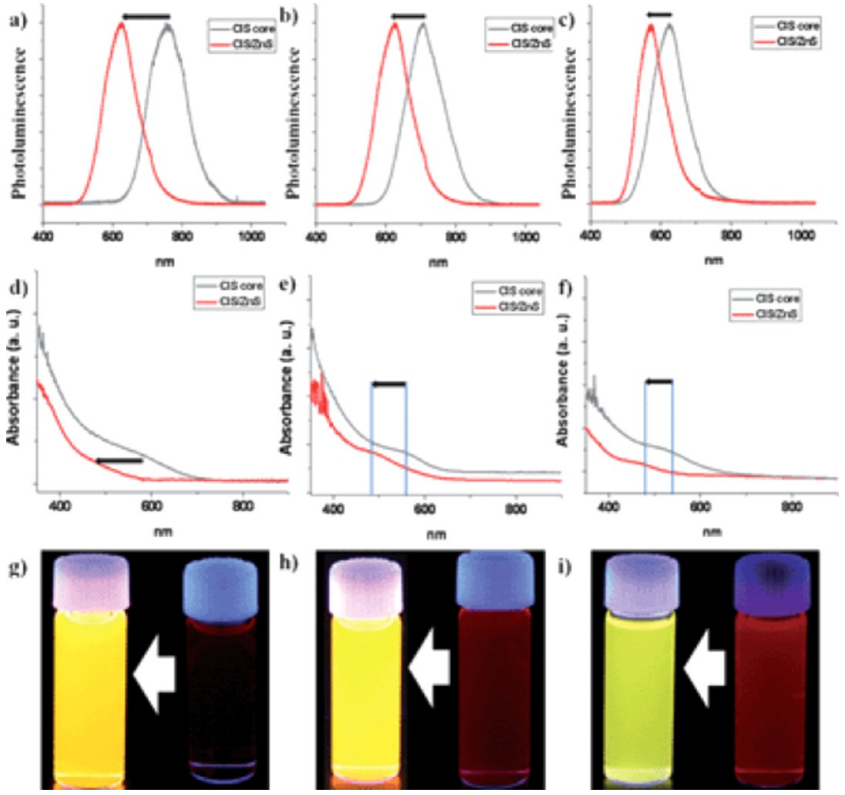

Figure 14. (a–c) PL and (d–f) absorption spectra of CIS particles with different sizes before and after reaction with Zn. (g–i) Digital photographs of the corresponding solutions under UV-irradiation. Reproduced with permission from ref 80. Copyright 2011 The Royal Society of Chemistry.

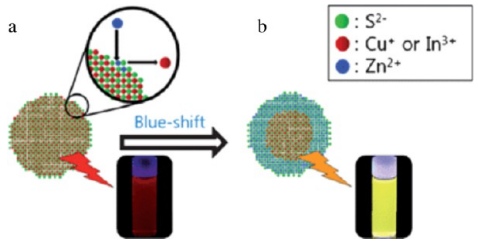

Figure 15. (a) Cation exchange in the CIS core upon addition of Zn^{2+} ions, leading to (b) the formation of a core–shell structure. Reproduced with permission from ref 80. Copyright 2011 The Royal Society of Chemistry.

vivid research activity in this field, no such improvement has been achieved, yet. Especially, problems related to the defects on the surface of the particles and the morphology of the active layer deteriorate the device performance. Efficiencies up to 5% could be achieved in devices using PbS, PbSe or CdSe nanocrystals;[128] in contrast, CIS nanocrystal blends with conducting polymers exhibit efficiencies far below 1%.[111]

Another possible device architecture for converting light into electricity is the so-called dye sensitized solar cell (DSSC). Light is absorbed in a dye covering a TiO_2 electrode and the photogenerated electrons are directly transferred to this electrode. The holes are transported with the help of a redox couple (typically I^- and I_3^-) through an organic electrolyte to the counter electrode. Efficiencies up to 11.4% could be achieved, when using a black ruthenium dye together with a co-sensitizer.[129] Also CIS-based materials are suitable light absorbing agents for this kind of devices. They have not only matching energy levels for charge separation (see also previous section) but also high extinction coefficients and radiation stability, which is superior, compared to organic dyes. In spite of these advantages, first devices fabricated with CIS nanocrystals instead of conventional dyes not only did not bring any improvement, but showed a substantially lower performance compared with DSSCs.[107] Some improvement could be achieved by covering CIS nanocrystals with a ZnS shell, but the efficiencies of the resulting devices still lay below 1%.[107] Further increase in the device performance (2.52% efficiency) was achieved by introducing a Cu_2S buffer layer[130] and by covering CIS nanocrystals with CdS. Optimization of the size of the nanocrystals and the thickness of the buffer layer led to efficiencies up to 4.2%,[131−133] whereas doping of the CdS layer with Mn yielded devices with 5.38% power conversion efficiency.[41] The positions of the energy levels of CdS and CIS can be adjusted by the size of the CIS core and the thickness of the CdS shell so, that a type II core–shell structure is formed. This spatially indirect energy gap facilitates the charge separation of the photogenerated charge carriers: the hole remains in the CIS core, whereas the electron is transferred to the shell. If CdS is doped with Mn, the electron gets trapped in the Mn $^4T_1$ state, which reduces the probability of charge recombination with holes and oxidized electrolyte. The electrons can be subsequently collected using an external circuit. This seems to be the reason for the higher power conversion efficiency of devices with Mn-doped CdS shells.[91] The drawback of this kind of architecture is the localization of the holes in the CIS-cores, which leads to less efficient extraction of these charge carriers.

The application of CIS nanoparticles as counter electrode in DSSCs was also reported.[91,134,135] Ligand-free (S^{2-} stabilized) CIS particles, which have a high surface area, showed good catalytic performance and high conductivity.[91] Films obtained

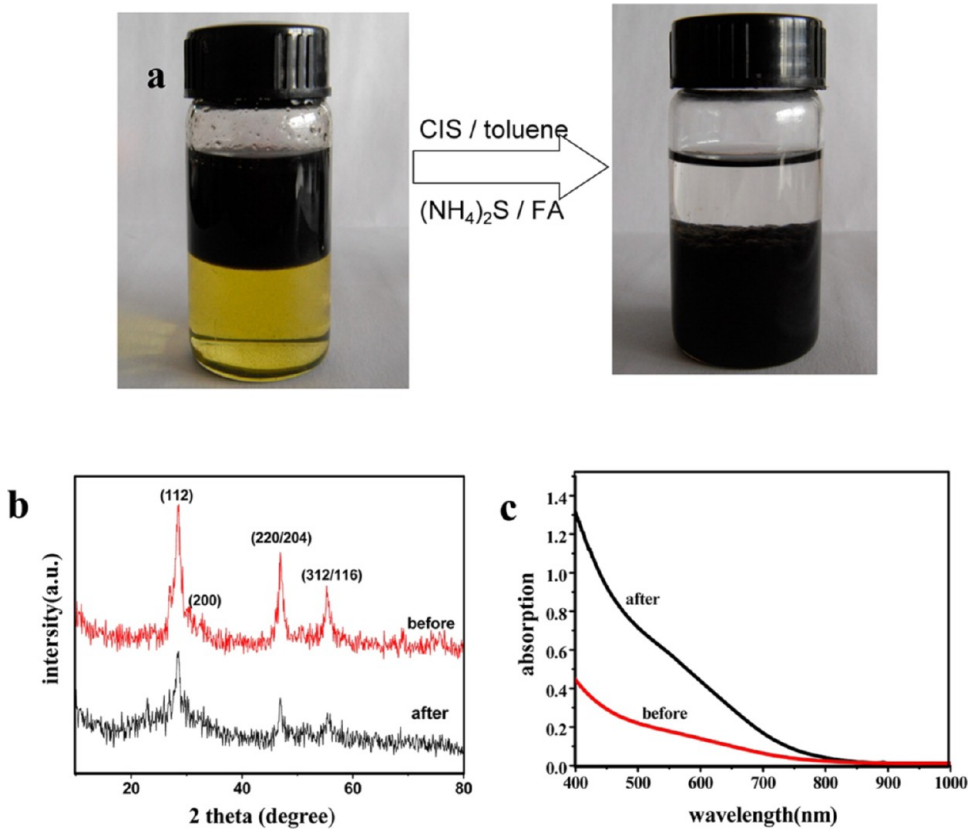

Figure 16. (a) Phase transfer of CIS nanoparticles from toluene to formamide upon exchange of the original organic surface ligands with S^{2-}. (b) Powder XRD patterns of CIS NCs before (red) and after (black) ligand removal. (c) Optical absorption spectra of CIS NCs before (red) and after (black) ligand removal. Reprinted with permission from ref 91. Copyright 2013 American Chemical Society.

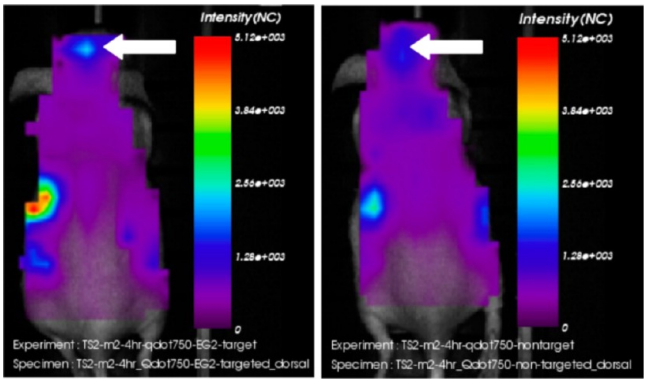

Figure 17. In vivo optical images demonstrate the biodistribution of the EG2 bioconjugated (left) and non-bioconjugated (right) CIS-ZnS NCs after their 4 h intravenous injection, as well as enhanced targeting of the bioconjugated CIS-ZnS NCs in an orthotopic brain glioblastoma tumor model, as compared by the intensity difference at the two sites pointed by the two arrows. The other bright spots correspond to excretion through the liver. Reprinted with permission from ref 92. Copyright 2013 American Chemical Society.

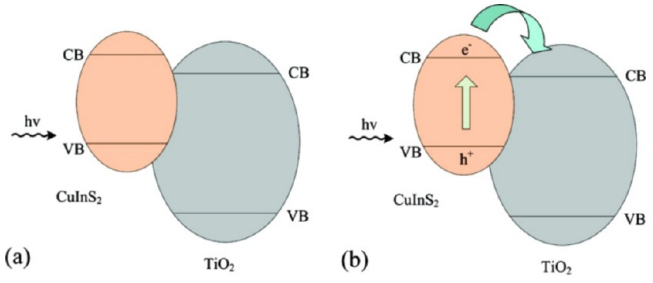

Figure 18. Schematic diagram of the photogenerated electron-hole separation process in CIS-TiO_2 particles, showing the system (a) before and (b) after light irradiation. Adapted with permission from ref 121. Copyright 2011 American Chemical Society.

by annealing of this ligand free nanocrystals, as well as vertically oriented CIS nanosheet thin films[134] and CIS-ZnS heterostructure nanorods,[135] show both power conversion efficiencies comparable to that of Pt electrodes (Figure 19).

3.4. Light-Emitting Diodes. The first report about the application of colloidal nanocrystals in light emitting diodes (LEDs) was published in 1994 by the Alivisatos group,[136] who observed electroluminescence of CdSe nanocrystals in a bilayer nanocrystals/polymer device. During the last 20 years, the brightness of nanocrystal-based LEDs improved by three orders of magnitude; furthermore, by using Pb or Hg chalcogenide nanocrystals, devices emitting in the IR spectral range could be obtained.[137] However, the search for less toxic and more environmentally friendly materials, which could replace cadmium, lead and mercury chalcogenides, did not give satisfactory results. Materials, such as colloidal Si, Ge, Ga, or In nitride and phosphide, or zinc chalcogenide nanocrystals did not show efficient electroluminescence. In contrast to this, the electroluminescence of CIS nanocrystals covered with a ZnS shell seems promising in view of their possible lighting application; furthermore, the large Stokes shifts of this kind of materials are advantageous for reducing self-absorption.[22,89,104,138−140]

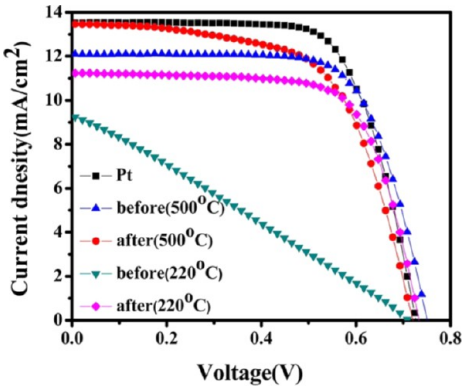

Figure 19. *J*–*V* characteristics of DSSCs with CIS before and after ligand exchange, annealed at different temperatures, and Pt as counter electrode. Reprinted with permission from ref 91. Copyright 2013 American Chemical Society.

Although the broad emission spectra of CIS-based materials are inadequate for applications requiring high degree of color purity, e.g., in display devices, this feature is especially suitable for producing white LEDs. Conventional white LEDs combine blue and yellow light to bichromatic white emission: a blue LED is covered by a phosphor, which emits yellow light upon blue excitation. However, the number of appropriate conventional phosphors with yellow emission, which can be excited by blue light, is rather limited. Furthermore, this kind of devices, containing micrometer-sized phosphors suffer from large scattering losses, reducing the luminous efficacy. This can be avoided by using nanocrystalline materials as color converters for LEDs, which not only show substantially less scattering, because of their small size, but also have the advantage of easily tunable emission wavelength.

In 2011, Tan et al.[139] demonstrated electroluminescence from alloyed CIS-ZnS nanocrystals, covered with a ZnSe/ZnS shell (Figure 20). The brightness of the resulting devices, emitting at red, yellow, and green wavelength (near band-edge emission of CIS-ZnS), was in the range between 1200 and 1600 cd/m^2. White light-emitting diodes were obtained by combining the red emission of CIS-ZnS nanocrystals with the blue-green emission of poly(N,N′-bis(4-butylphenyl)-N,N′-bis(phenyl)benzidine (poly-TPD) in a bilayer device.[140] The Commission Internationale de l'Eclairage (CIE) chromacity coordinates of the resulting device were (0.336, 0339), which is close to the balanced white coordinates (0.333, 0.333), and it exhibited a relatively high color rendering index (CRI) of 92 (CRI values above 80 are acceptable for indoor lighting applications). However, the stability of the device was not satisfactory, because of the rapid degradation of the organic material, which led to a shift of the CIE coordinates towards the red region. CIS and Cu–In–Ga-S nanocrystals covered with a ZnS shell were also successfully applied as color converter in white LEDs based on InGaN blue-emitting LEDs.[89,104,138] Song et al. adjusted the emission properties of CIS-ZnS core-shell nanocrystals by changing the ratio between copper and indium.[89] They obtained white light with CIS coordinates of (0.347, 0.288) and CRI of 72 and a luminous efficiency of 63.4 lm/W by mixing of the blue light of a LED and yellow emitting nanocrystals (Cu:In ratio of 1:4) (Figure 21). The position of the emission of CIS nanocrystals can be also adjusted by alloying this material with $CuGaS_2$. LEDs with ZnS-coated Cu-In_{1-x}-Ga_x-S nanoparticles exhibited luminous efficacies between

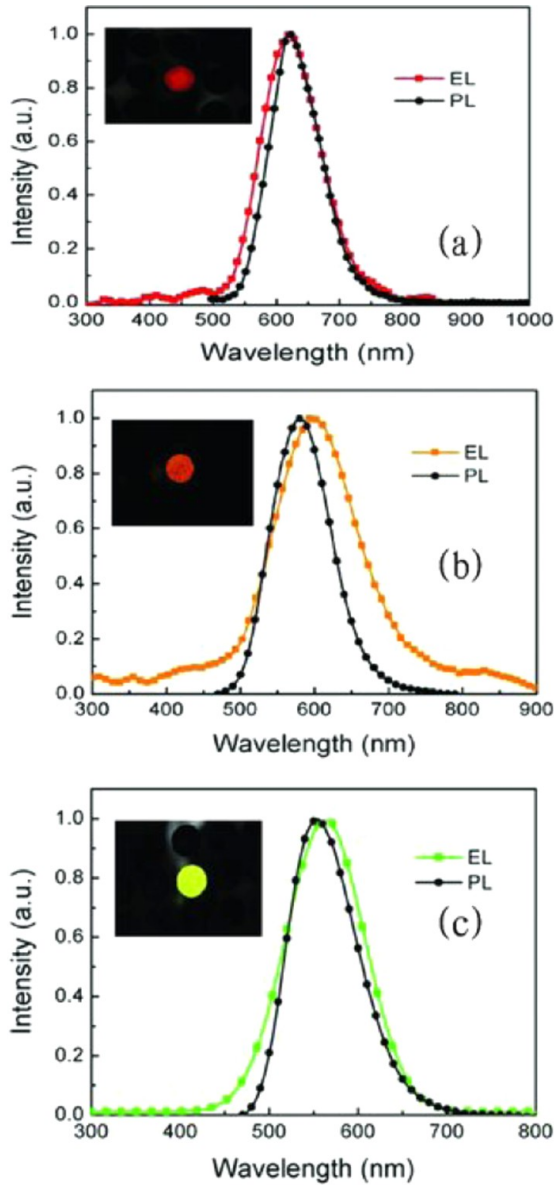

Figure 20. Electroluminescence (EL) and photoluminescence (PL) of CIS-ZnS nanocrystals of different sizes: (a) 3.3, (b) 2.7, and (c) 2.3 nm. The insets show digital photographs of the corresponding LEDs. Reprinted with permission from ref 139. Copyright 2011 Wiley–VCH.

69.1 and 75.0 lm/W and CRI values of 71–72. Higher CRI values (76-78) were obtained by using two different kinds of nanoparticles, with a broader spectral coverage, as color converterts.[104]

SUMMARY AND OUTLOOK

CIS is a material with low toxicity and interesting optical properties. Colloidal synthesis of CIS nanocrystals strongly developed during the last decade, which rendered possible a variety of applications of this material, e.g., in biolabelling, photocatalysis, solar energy conversion, display technology, or light-emitting diodes. However, the optical properties of this material are not yet understood in detail. They have to be investigated further to shed light onto the origin of some contradictory explanations that can be found in the literature. When comparing different studies of the properties of CIS nanocrystals one has to keep in mind that its properties do not

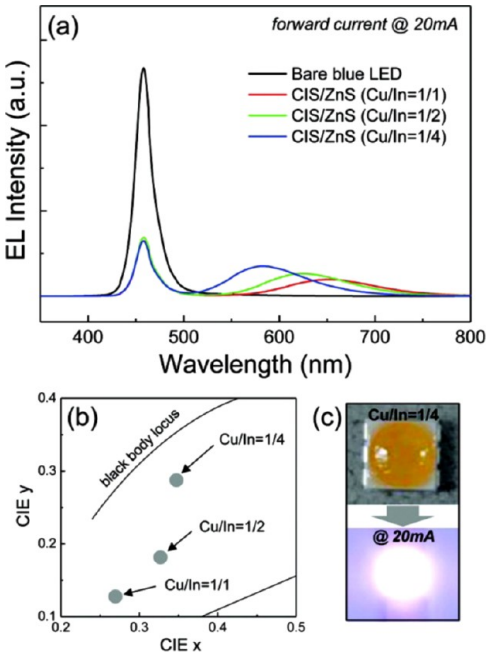

Figure 21. (a) Electroluminescence spectra and (b) CIE color coordinates of LEDs combined with Cu/In = 1/1-, 1/2-, and 1/4-based CIS-ZnS nanocrystals under a forward current of 20 mA. (c) Photographs of white LED fabricated with Cu/In = 1/4-based CIS-ZnS nanocrystals before and after the application of a forward current of 20 mA. Reprinted with permission from ref 89. Copyright 2012 American Chemical Society.

depend only on the size, shape and crystallographic structure of the crystallites, but are also strongly influenced by their composition. Because of the pronounced defect tolerance of this material its stoichiometry can be varied in a wide range and strongly depends on the exact conditions of the synthesis. Therefore, our understanding of the processes taking place during the synthesis and of the growth process of CIS nanocrystals also has to be further extended, in order to gain precise control over the size-, shape-, and composition-dependent properties of this material and to fully exploit its application potential.

AUTHOR INFORMATION

Corresponding Author

*E-mail: joanna.kolny@uni-oldenburg.de.

Author Contributions

The manuscript was written through contributions of all authors. All authors have given approval to the final version of the manuscript.

Notes

The authors declare no competing financial interest.

ACKNOWLEDGMENTS

We gratefully acknowledge funding of the EWE Research Group "Thin Film Photovoltaics" by the EWE AG, Oldenburg.

REFERENCES

(1) Murray, C. B.; Kagan, C. R.; Bawendi, M. G. *Annu. Rev. Mater. Sci.* **2000**, *30*, 545−610.
(2) Weller, H. *Angew. Chem.* **1993**, *105*, 43−55.
(3) Alivisatos, P. *J. Phys. Chem.* **1996**, *100*, 13226−13239.
(4) Burda, C.; Chen, X.; Narayanan, R.; El-Sayed, M. a. *Chem. Rev.* **2005**, *105*, 1025−102.
(5) Cozzoli, P. D.; Pellegrino, T.; Manna, L. *Chem. Soc. Rev.* **2006**, *35*, 1195−208.
(6) Rogach, A. L.; Eychmüller, A.; Hickey, S. G.; Kershaw, S. V *Small* **2007**, *3*, 536−557.
(7) Park, J.; Joo, J.; Kwon, S. G. G.; Jang, Y.; Hyeon, T. *Angew. Chem., Int. Ed.* **2007**, *46*, 4630−4660.
(8) Sowers, K. L.; Swartz, B.; Krauss, T. D. *Chem. Mater.* **2013**, *25*, 1351−1362.
(9) Mourdikoudis, S.; Liz-Marzán, L. *Chem. Mater.* **2013**, *25*, 14665−1476.
(10) Reiss, P.; Protière, M.; Li, L. *Small* **2009**, *5*, 154−168.
(11) Kumar, S.; Nann, T. *Small* **2006**, *2*, 316−329.
(12) Owen, J. S.; Chan, E. M.; Liu, H.; Alivisatos, P. *J. Am. Chem. Soc.* **2010**, *132*, 18206−18213.
(13) Owen, J. S.; Park, J.; Trudeau, P.-E.; Alivisatos, P. *J. Am. Chem. Soc.* **2008**, *130*, 12279−12281.
(14) García-Rodríguez, R.; Hendricks, M. P.; Cossairt, B. M.; Liu, H.; Owen, J. S. *Chem. Mater.* **2013**, *25*, 1233−1249.
(15) García-Rodríguez, R.; Liu, H. *J. Am. Chem. Soc.* **2012**, *134*, 1400−1403.
(16) Yu, K.; Liu, X.; Zeng, Q.; Leek, D. M.; Ouyang, J.; Whitmore, K. M.; Ripmeester, J. a; Tao, Y.; Yang, M. *Angew. Chem. Int. Ed. Engl.* **2013**, *52*, 4823−4828.
(17) Zhao, Y.; Burda, C. *Energy Environ. Sci* **2012**, *5*, 5564−5576.
(18) Witt, E.; Kolny-Olesiak, J. *Chem.—Eur. J.* **2013**, *19*, 9746−9753.
(19) Aldakov, D.; Lefrançois, A.; Reiss, P. *J. Mater. Chem. C* **2013**, *1*, 3756−3776.
(20) Omata, T.; Nose, K.; Otsuka-Yao-Matsuo, S. *J. Appl. Phys.* **2009**, *105*, 073106.
(21) Uehara, M.; Watanabe, K.; Tajiri, Y.; Nakamura, H.; Maeda, H. *J. Chem. Phys.* **2008**, *129*, 134709.
(22) Chen, B.; Zhong, H.; Zhang, W.; Tan, Z.; Li, Y.; Yu, C.; Zhai, T.; Bando, Y.; Yang, S.; Zou, B. *Adv. Funct. Mater.* **2012**, *22*, 2081−2088.
(23) Xie, R.; Rutherford, M.; Peng, X. *J. Am. Chem. Soc.* **2009**, *131*, 5691−5697.
(24) Castro, S. L.; Bailey, S. G.; Raffaelle, R. P.; Banger, K. K.; Hepp, A. F. *J. Phys. Chem. B* **2004**, *108*, 12429−12435.
(25) Booth, M.; Brown, A.; Evans, S.; Critchley, K. *Chem. Mater.* **2012**, *24*, 2064−2070.
(26) Qin, L.; Li, D.; Zhang, Z.; Wang, K.; Ding, H.; Xie, R.; Yang, W. *Nanoscale* **2012**, *4*, 6360−6364.
(27) Niezgoda, J.; Harrison, M. *Chem. Mater.* **2012**, *24*, 3294−3298.
(28) Li, L.; Daou, T. J. T.; Texier, I.; Chi, T. K.; Kim Chi, T. T.; Liem, N. Q.; Reiss, P. *Chem. Mater.* **2009**, *21*, 2422−2429.
(29) Nairn, J. J.; Shapiro, P. J.; Twamley, B.; Pounds, T.; Wandruszka, R.; von Fletcher, T. R.; Williams, M.; Wang, C.; Norton, M. G. *Nano Lett.* **2006**, *6*, 1218−1223.
(30) Trizio, L.; De Prato, M.; Genovese, A.; Casu, A.; Povia, M.; Simonutti, R.; Alcocer, M. J. P.; Andrea, C. D.; Tassone, F.; Manna, L. *Chem. Mater.* **2012**, *24*, 2400−2406.
(31) Hamanaka, Y.; Kuzuya, T.; Sofue, T.; Kino, T.; Ito, K.; Sumiyama, K. *Chem. Phys. Lett.* **2008**, *466*, 176−180.
(32) Pan, D.; Weng, D.; Wang, X.; Xiao, Q.; Chen, W.; Xu, C.; Yang, Z.; Lu, Y. *Chem. Commun.* **2009**, *28*, 4221−4223.
(33) Li, L.; Pandey, A.; Werder, D. J.; Khanal, B. P.; Pietryga, J. M.; Klimov, V. I. *J. Am. Chem. Soc.* **2011**, *133*, 1176−1179.
(34) Castro, S. L.; Bailey, S. G.; Raffaelle, R. P.; Banger, K. K.; Hepp, A. F. *Chem. Mater.* **2003**, *15*, 3142−3147.
(35) Batabyal, S. K.; Tian, L.; Venkatram, N.; Ji, W.; Vittal, J. J. *J. Phys. Chem. C* **2009**, *113*, 15037−15042.
(36) Bensebaa, F.; Durand, C.; Aouadou, A.; Scoles, L.; Du, X.; Wang, D.; Page, Y. *J. Nanoparticle Res.* **2009**, 1897−1903.
(37) Liu, Q.; Zhao, Z.; Lin, Y.; Guo, P.; Li, S.; Pan, D.; Ji, X. *Chem. Commun.* **2011**, *47*, 964−966.
(38) Liu, S.; Zhang, H.; Qiao, Y.; Su, X. *RSC Adv.* **2012**, *2*, 819−825.

(39) Wang, M.; Liu, X.; Cao, C.; Shi, C. *RSC Adv.* **2012**, *2*, 2666−2670.
(40) Chen, Y.; Li, S.; Huang, L.; Pan, D. *Inorg. Chem.* **2013**, *52*, 7819−7821.
(41) Luo, J.; Wei, H.; Huang, Q.; Hu, X.; Zhao, H.; Yu, R.; Li, D.; Luo, Y.; Meng, Q. *Chem. Commun.* **2013**, *49*, 3881−3883.
(42) Czekelius, C.; Hilgendorff, M.; Spanhel, L.; Bedja, I.; Lerch, M.; Müller, G.; Bloeck, U.; Su, D.-S.; Giersig, M. *Adv. Mater.* **1999**, *11*, 643−646.
(43) Jiang, Y.; Wu, Y.; Mo, X.; Yu, W.; Xie, Y.; Qian, Y. *Inorg. Chem.* **2000**, *39*, 2964−2965.
(44) Lu, Q.; Hu, J.; Tang, K.; Qian, Y.; Zhou, G.; Liu, X. *Inorg. Chem.* **2000**, *39*, 1606−1607.
(45) Cui, Y.; Ren, J.; Chen, G.; Qian, Y.; Xie, Y. *Chem. Lett.* **2001**, *2*, 236−237.
(46) Dutta, D. P.; Sharma, G. *Mater. Lett.* **2006**, *60*, 2395−2398.
(47) Nakamura, H.; Kato, W.; Uehara, M.; Nose, K.; Omata, T.; Otsuka-Yao-Matsuo, S.; Miyazaki, M.; Maeda, H. *Chem. Mater.* **2006**, *18*, 3330−3335.
(48) Du, W.; Qian, X.; Yin, J.; Gong, Q. *Chem.—Eur. J.* **2007**, *13*, 8840−8846.
(49) Gardner, J. S.; Shurdha, E.; Wang, C.; Lau, L. D.; Rodriguez, R. G.; Pak, J. J. *J. Nanoparticle Res.* **2007**, *10*, 633−641.
(50) Kino, T.; Kuzuya, T.; Itoh, K.; Sumiyama, K.; Wakamatsu, T.; Ichidate, M. *Mater. Trans.* **2008**, *49*, 435−438.
(51) Pan, D.; An, L.; Sun, Z.; Hou, W.; Yang, Y.; Yang, Z.; Lu, Y. *J. Am. Chem. Soc.* **2008**, *130*, 5620−5621.
(52) Panthani, M. G.; Akhavan, V.; Goodfellow, B.; Schmidtke, J. P.; Dunn, L.; Dodabalapur, A.; Barbara, P. F.; Korgel, B. A. *J. Am. Chem. Soc.* **2008**, *130*, 16770−16777.
(53) Wang, D.; Zheng, W.; Hao, C.; Peng, Q.; Li, Y. *Chem. Commun.* **2008**, 2556−2558.
(54) Zhang, A.; Ma, Q.; Lu, M.; Yu, G.; Zhou, Y.; Qiu, Z. *Cryst. Growth Des.* **2008**, *8*, 2402−2405.
(55) Zhong, H.; Zhou, Y.; Ye, M.; He, Y.; Ye, J.; He, C.; Yang, C.; Li, Y. *Chem. Mater.* **2008**, *20*, 6434−6443.
(56) Connor, S. T.; Hsu, C.-M.; Weil, B. D.; Aloni, S.; Cui, Y. *J. Am. Chem. Soc.* **2009**, *131*, 4962−4966.
(57) Courtel, F. M.; Paynter, R. W.; Marsan, B.; Morin, M. *Chem. Mater.* **2009**, *21*, 3752−3762.
(58) Koo, B.; Patel, R. N.; Korgel, B. a. *Chem. Mater.* **2009**, *21*, 1962−1966.
(59) Norako, M. E.; Franzman, M. a.; Brutchey, R. L. *Chem. Mater.* **2009**, *21*, 4299−4304.
(60) Nose, K.; Soma, Y.; Omata, T.; Otsuka-Yao-Matsuo, S. *Chem. Mater.* **2009**, *21*, 2607−2613.
(61) Sun, C.; Gardner, J. S.; Shurdha, E.; Margulieux, K. R.; Westover, R. D.; Lau, L.; Long, G.; Bajracharya, C.; Wang, C.; Thurber, A.; Punnoose, A.; Rodriguez, R. G.; Pak, J. J. *J. Nanomater.* **2009**, *2009*, 748567.
(62) Qi, Y.; Liu, Q.; Tang, K.; Liang, Z.; Ren, Z.; Liu, X. *J. Phys. Chem. C* **2009**, *113*, 3939−3944.
(63) Kruszynska, M.; Borchert, H.; Parisi, J.; Kolny-Olesiak, J. *J. Am. Chem. Soc.* **2010**, *132*, 15976−15986.
(64) Li, T.-L.; Teng, H. *J. Mater. Chem.* **2010**, *20*, 3656−3664.
(65) Pons, T.; Pic, E.; Lequeux, N.; Cassette, E.; Bezdetnaya, L.; Guillemin, F.; Marchal, F.; Dubertret, B. *ACS Nano* **2010**, *4*, 2531−2538.
(66) Shi, L.; Pei, C.; Li, Q. *Nanoscale* **2010**, *2*, 2126−2130.
(67) Sun, C.; Gardner, J. S.; Long, G.; Bajracharya, C.; Thurber, A.; Punnoose, A.; Rodriguez, R. G.; Pak, J. J. *Chem. Mater.* **2010**, *22*, 2699−2701.
(68) Yong, K.-T.; Roy, I.; Hu, R.; Ding, H.; Cai, H.; Zhu, J.; Zhang, X.; Bergey, E. J.; Prasad, P. N. *Integr. Biol.* **2010**, *2*, 121−129.
(69) Yue, W.; Han, S.; Peng, R.; Shen, W.; Geng, H.; Wu, F.; Tao, S.; Wang, M. *J. Mater. Chem.* **2010**, *20*, 7570.
(70) Zhong, H.; Lo, S. S.; Mirkovic, T.; Li, Y.; Ding, Y.; Li, Y.; Scholes, G. D. *ACS Nano* **2010**, *4*, 5253−5262.
(71) Bao, N.; Qiu, X.; Wang, Y.-H. a; Zhou, Z.; Lu, X.; Grimes, C. a.; Gupta, A. *Chem. Commun.* **2011**, *47*, 9441−9443.
(72) Chiang, M. Y.; Chang, S.; Chen, C. Y.; Yuan, F. W.; Tuan, H. Y. *J. Phys. Chem. C* **2011**, *115*, 1592−1599.
(73) Courtel, F. M.; Hammami, A.; Imbeault, R.; Hersant, G.; Paynter, R. W.; Marsan, B.; Morin, M. *Chem. Mater.* **2010**, *22*, 3752−3761.
(74) Kruszynska, M.; Borchert, H.; Parisi, J.; Kolny-Olesiak, J. *J. Nanoparticle Res.* **2011**, *13*, 5815−5824.
(75) Luo, Y.; Chang, G.; Lu, W.; Sun, X. *Colloid J.* **2010**, *72*, 282−285.
(76) Liu, H.-T.; Zhong, J.-S.; Liu, B.-F.; Liang, X.-J.; Yang, X.-Y.; Jin, H.-D.; Yang, F.; Xiang, W.-D. *Chinese Phys. Lett.* **2011**, *28*, 057702.
(77) Lu, X.; Zhuang, Z.; Peng, Q.; Li, Y. *CrystEngComm* **2011**, *13*, 4039−4045.
(78) Nam, D.-E.; Song, W.-S.; Yang, H. *J. Colloid Interface Sci.* **2011**, *361*, 491−496.
(79) Nam, D.-E.; Song, W.-S.; Yang, H. *J. Mater. Chem.* **2011**, *21*, 18220−18226.
(80) Park, J.; Kim, S.-W. *J. Mater. Chem.* **2011**, *21*, 3745−3750.
(81) Pein, A.; Baghbanzadeh, M.; Rath, T.; Haas, W.; Maier, E.; Amenitsch, H.; Hofer, F.; Kappe, C. O.; Trimmel, G. *Inorg. Chem.* **2011**, *50*, 193−200.
(82) Sheng, X.; Wang, L.; Luo, Y.; Yang, D. *Nanoscale Res. Lett.* **2011**, *6*, 562.
(83) Tang, X.; Cheng, W.; Choo, E. S. G.; Xue, J. *Chem. Commun.* **2011**, 5217−5219.
(84) Abdelhady, A. L.; Malik, M. a.; O'Brien, P. *J. Mater. Chem.* **2012**, *22*, 3781−3785.
(85) Deng, D.; Chen, Y.; Cao, J.; Tian, J.; Qian, Z.; Achilefu, S.; Gu, Y. *Chem. Mater.* **2012**, *24*, 3029−3037.
(86) He, J.-J.; Zhou, W.-H.; Guo, J.; Li, M.; Wu, S.-X. *CrystEngComm* **2012**, *14*, 3638−3644.
(87) Huang, W.; Tseng, C.; Chang, S.; Tuan, H.; Chiang, C.-C.; Lyu, L.-M.; Huang, M. H. *Langmuir* **2012**, *28*, 8496−8501.
(88) Sheng, X.; Wang, L.; Yang, D. *J. Sol−Gel Sci. Technol.* **2012**, *62*, 87−91.
(89) Song, W.; Yang, H. *Chem. Mater.* **2012**, *24*, 1961−1967.
(90) Chang, J.; Waclawik, E. *CrystEngComm* **2013**, *15*, 5612−5619.
(91) Yao, R.-Y.; Zhou, Z.-J.; Hou, Z.-L.; Wang, X.; Zhou, W.-H.; Wu, S.-X. *ACS Appl. Mater. Interfaces* **2013**, *5*, 3143−3148.
(92) Yu, K.; Ng, P.; Ouyang, J.; Badruz Zaman, M.; Abulrob, A.; Baral, T. N.; Fetehi, D.; Jakubek, Z. J.; Kingston, D.; Wu, X.; Liu, X.; Hebert, C.; Leek, D. M.; Whitfield, D. M. *ACS Appl. Mater. Interfaces* **2013**, *5*, 2870−2880.
(93) Binsma, J. J. M.; Giling, L. J.; Bloem, J. *J. Cryst. Growth* **1980**, *50*, 429−436.
(94) Kuzuya, T.; Hamanaka, Y.; Itoh, K.; Kino, T.; Sumiyama, K.; Fukunaka, Y.; Hirai, S. *J. Colloid Interface Sci.* **2012**, *388*, 137−143.
(95) Li, Q.; Zhai, L.; Zou, C.; Huang, X.; Zhang, L.; Yang, Y.; Chen, X.; Huang, S. *Nanoscale* **2013**, *5*, 1638−1648.
(96) Li, Q.; Zou, C.; Zhai, L.; Zhang, L.; Yang, Y.; Chen, X.; Huang, S. *CrystEngComm* **2013**, *15*, 1806−1813.
(97) Zhang, W.; Zhong, X. *Inorg. Chem.* **2011**, *50*, 4065−4072.
(98) Ye, C.; Regulacio, M. D.; Lim, S. H.; Xu, Q.-H.; Han, M.-Y. *Chem. A Eur. J.* **2012**, *18*, 11258−11263.
(99) Chang, J.-Y.; Cheng, C.-Y. *Chem. Commun.* **2011**, *47*, 9089−9091.
(100) Zhang, J.; Xie, R. *Chem. Mater.* **2011**, *23*, 3357−3361.
(101) Feng, J.; Sun, M.; Yang, F.; Yang, X. *Chem. Commun.* **2011**, *47*, 6422−6424.
(102) Guijarro, N.; Lana-Villarreal, T.; Gómez, R. *Chem. Commun.* **2012**, *48*, 7681−7683.
(103) Wang, X.; Pan, D.; Weng, D.; Low, C. Y. C.-Y.; Rice, L.; Han, J.; Lu, Y. *J. Phys. Chem. C* **2010**, *114*, 13406−13413.
(104) Song, W.-S.; Kim, J.-H.; Lee, J.-H.; Lee, H.-S.; Do, Y. R.; Yang, H. *J. Mater. Chem.* **2012**, *22*, 21901.
(105) Wang, Y.-H. a; Zhang, X.; Bao, N.; Lin, B.; Gupta, A. *J. Am. Chem. Soc.* **2011**, *133*, 11072−11075.

(106) Bose, R.; Jana, S.; Manna, G.; Chakraborty, S.; Pradhan, N. *J. Phys. Chem. C* **2013**, *117*, 15835−15841.
(107) Kuo, K.-T.; Liu, D.-M.; Chen, S.-Y.; Lin, C.-C. *J. Mater. Chem.* **2009**, *19*, 6780−6788.
(108) Pan, H.-J.; Lai, C.-W.; Chou, S.-W.; Chou, P.-T. *Mater. Express* **2012**, *2*, 224−232.
(109) Guo, W.; Chen, N.; Tu, Y.; Dong, C.; Zhang, B.; Hu, C.; Chang, J. *Theranostics* **2013**, *3*, 99−108.
(110) Wang, M.; Liu, X.; Cao, C.; Wang, L. *J. Mater. Chem.* **2012**, *22*, 21979−21986.
(111) Radychev, N.; Scheunemann, D.; Kruszynska, M.; Frevert, K.; Miranti, R.; Kolny-Olesiak, J.; Borchert, H.; Parisi, J. *Org. Electron.* **2012**, *13*, 3154−3164.
(112) Mandal, G.; Darragh, M.; Wang, Y. A.; Heyes, C. D. *Chem. Commun.* **2013**, *49*, 624−626.
(113) Zhong, H.; Bai, Z.; Zou, B. *J. Phys. Chem. Lett.* **2012**, *3*, 3167−3175.
(114) Permadi, A.; Fahmi, M. Z.; Chen, J.-K.; Chang, J.-Y.; Cheng, C.-Y.; Wang, G.-Q.; Ou, K.-L. *RSC Adv.* **2012**, *2*, 6018−6022.
(115) Manna, G.; Jana, S.; Bose, R.; Pradhan, N. *J. Phys. Chem. Lett.* **2012**, *3*, 2528−2534.
(116) Li, T.-L.; Cai, C.-D.; Yeh, T.-F.; Teng, H. *J. Alloys Compd.* **2013**, *550*, 326−330.
(117) Nag, A.; Kovalenko, M. V; Lee, J.-S.; Liu, W.; Spokoyny, B.; Talapin, D. V *J. Am. Chem. Soc.* **2011**, *133*, 10612−10620.
(118) Kovalenko, M. V; Scheele, M.; Talapin, D. V *Science* **2009**, *324*, 1417−1420.
(119) Cheng, C.-Y.; Ou, K.-L.; Huang, W.-T.; Chen, J.-K.; Chang, J.-Y.; Yang, C.-H. *ACS Appl. Mater. Interfaces* **2013**, *5*, 4389−4400.
(120) Lin, Y.; Zhang, F.; Pan, D.; Li, H.; Lu, Y. *J. Mater. Chem.* **2012**, *22*, 8759−8763.
(121) Shen, F.; Que, W.; Liao, Y.; Yin, X. *Ind. Eng. Chem. Res.* **2011**, *50*, 9131−9137.
(122) Zheng, L.; Xu, Y.; Song, Y.; Wu, C.; Zhang, M.; Xie, Y. *Inorg. Chem.* **2009**, *48*, 4003−4009.
(123) Tsuji, I.; Kato, H.; Kobayashi, H.; Kudo, A. *J. Phys. Chem. B* **2005**, *2*, 7323−7329.
(124) Green, M. A.; Emery, K.; Hishikawa, Y.; Warta, W.; Dunlop, E. D. *Prog. Photovolt. Res. Appl.* **2013**, *21*, 1−11.
(125) Habas, S. E.; Platt, H. A. S.; van Hest, M. F. A. M.; Ginley, D. S. *Chem. Rev.* **2010**, *110*, 6571−6594.
(126) Li, L.; Coates, N.; Moses, D. *J. Am. Chem. Soc.* **2009**, *132*, 22−23.
(127) He, Z.; Zhong, C.; Huang, X.; Wong, W.-Y.; Wu, H.; Chen, L.; Su, S.; Cao, Y. *Adv. Mater.* **2011**, *23*, 4636−4643.
(128) Zhou, R.; Xue, J. *ChemPhysChem* **2012**, *13*, 2471−2480.
(129) Han, L.; Islam, A.; Chen, H.; Malapaka, C.; Chiranjeevi, B.; Zhang, S.; Yang, X.; Yanagida, M. *Energy Environ. Sci.* **2012**, *5*, 6057−6060.
(130) Chang, J.-Y.; Su, L.-F.; Li, C.-H.; Chang, C.-C.; Lin, J.-M. *Chem. Commun.* **2012**, *48*, 4848−4850.
(131) Li, T.-L.; Lee, Y.-L.; Teng, H. *Energy Environ. Sci.* **2012**, *5*, 5315−5324.
(132) Li, T.-L.; Lee, Y.-L.; Teng, H. *J. Mater. Chem.* **2011**, *21*, 5089−5098.
(133) Santra, P. K.; Nair, P. V.; Thomas, K. G.; Kamat, P. V. *J. Phys. Chem. Lett.* **2013**, *4*, 722−729.
(134) Yang, J.; Bao, C.; Zhang, J.; Yu, T.; Huang, H.; Wei, Y.; Gao, H.; Fu, G.; Liu, J.; Zou, Z. *Chem. Commun.* **2013**, *49*, 2028−2030.
(135) Yi, L.; Liu, Y.; Yang, N.; Tang, Z.; Zhao, H.; Ma, G.; Su, Z.; Wang, D. *Energy Environ. Sci.* **2013**, *6*, 835−840.
(136) Colvin, V.; Schlamp, M.; Alivisatos, A. *Nature* **1994**, *370*, 354−357.
(137) Rogach, A. L.; Gaponik, N.; Lupton, J. M.; Bertoni, C.; Gallardo, D. E.; Dunn, S.; Li Pira, N.; Paderi, M.; Repetto, P.; Romanov, S. G.; O'Dwyer, C.; Sotomayor Torres, C. M.; Eychmüller, A. *Angew. Chem., Int. Ed.* **2008**, *47*, 6538−6549.
(138) Chen, B.; Zhou, Q.; Li, J.; Zhang, F.; Liu, R.; Zou, B. *Opt. Express* **2013**, *21*, 10105−10110.
(139) Tan, Z.; Zhang, Y.; Xie, C.; Su, H.; Liu, J.; Zhang, C.; Dellas, N.; Mohney, S. E.; Wang, Y.; Wang, J.; Xu, J. *Adv. Mater.* **2011**, *23*, 3553−3558.
(140) Zhang, Y.; Xie, C.; Su, H.; Liu, J.; Pickering, S.; Wang, Y.; Yu, W. W.; Wang, J.; Wang, Y.; Hahm, J.; Dellas, N.; Mohney, S. E.; Xu, J. *Nano Lett.* **2011**, *11*, 329−332.